

1 **The role of late Quaternary tectonic activity and sea-level changes on sedimentary**
2 **processes interaction in the Gulf of Cadiz upper and middle continental slope (SW Iberia)**

3 García, M.^{1,2,*}, Llave, E.³, Hernández-Molina, F.J.⁴, Lobo, F.J.², Ercilla, G.⁵, Alonso, B.⁵, Casas, D.⁵, Mena,
4 A.⁶, Fernández-Salas, L.M.¹

5 ¹ Spanish Institute of Oceanography, Centre of Cadiz. Muelle Pesquero s/n, Cadiz. marga.garcia@ieo.es
6 (*corresponding author); luismi.fernandez@ieo.es.

7 ² Andalusian Institute of Earth Sciences, CSIC-UGR. Avda. de las Palmeras 4, Armilla (Granada).
8 francisco.lopez@csic.es.

9 ³ Spanish Geological Survey. C/ La Calera, 1, Tres Cantos (Madrid). e.llave@igme.es.

10 ⁴ Department of Earth Sciences, Royal Holloway University of London. Egham Hill, Egham TW20 0EX,
11 UK. Javier.Hernandez-Molina@rhul.ac.uk.

12 ⁵ Institute of Marine Sciences, CSIC. Passeig Marítim de la Barceloneta, 37-49. Barcelona.
13 gemma@icm.csic.es; belen@icm.csic.es; davidcasas@icm.csic.es.

14 ⁶ Department of Marine Geosciences and Land Management, University of Vigo. CUVI, Vigo.
15 anxomena@uvigo.es.

16 **Abstract**

17 A morphological and seismic-stratigraphic analysis of the Gulf of Cadiz area near the Strait of
18 Gibraltar is presented in this work, focused on the sedimentary evolution of the upper and proximal
19 middle-continental slope since the Mid-Pleistocene. Based on the analysis of seismic reflection profiles
20 and swath bathymetry data, this work analyses the close influence of the activity of buried and
21 outcropping diapiric ridges and late Quaternary sea-level changes on the evolution of contouritic
22 features related to the Mediterranean Outflow Water (MOW) and Eastern North Atlantic Central
23 Water (ENACW), gravitational features and fluid-escape structures. The stratigraphic architecture
24 reveals that, under active diapiric deformation, the upper slope plastered drift grew during low sea-
25 level stages, when sediment supply was high and the ENACW swept the upper slope, contrasting with
26 the present-day highstand situation dominated by northwest-trending MOW flow. The south-estward
27 ENACW flow forced asymmetry and lateral migration of gullies incised in the plastered drift. Two
28 evolutionary stages have been established: 1) After the Mid Pleistocene, activity of diapirs with a NE
29 trend determined the location of the deepest depressions which were infilled by plastered contouritic
30 drifts; 2) Between Late Quaternary and present, a drastic change of buried diapirs growth pattern and
31 orientation to a NW trend enhanced slope-derived gravitational processes affecting the bottom
32 current dynamics. Adjustments to tectonic changes led to a phase of plastered drift growth on the
33 upper slope during which depocenters varied their distribution and orientation. In a long-term the
34 structural control on sedimentation shows a northwestward displacement of deformation, resulting in
35 an overall extension of the contourite depositional system to the NW. In a short-term, sea-level
36 changes favoured drift deposition, gullies incision and the strengthening of water masses. This work
37 evidences the importance of tectonic deformation in sedimentation at recent time scales, and the two-
38 directional interplay between recent tectonic activity and bottom current dynamics.

39

40 **Keywords:** Tectonics; Sea-level; Diapirs; Contourites; Gullies; Seismic stratigraphy; Continental slope;
41 Gulf of Cadiz.

42 **1. Introduction**

43 Sedimentary processes in siliciclastic continental margins are controlled by the interactions of
44 regional basin tectonics, sea-level fluctuations and sediment supply (Haq et al., 1987; Richards et al.,
45 1998). In fact, tectonism may in the long term control climate and sea-level (Mack, 1978). Under this
46 ultimate control, numerous sedimentary processes interplay in shaping continental margins (Nelson
47 and Maldonado, 1988; Viana, 2009; Shanmugan, 2012). A growing body of evidence indicates that
48 interactions between downslope gravitational processes and along-slope oceanographic processes are
49 ubiquitous in numerous deep-water settings (Howe, 1996; Gong et al., 2013; Fongnesu et al., 2020) and
50 that they are of high importance in terms of hydrocarbon potential (Rodríguez and Hodgson, 2019).
51 The interactions between turbidity flows and contour currents may be coeval (Mulder et al., 2008;
52 Ercilla et al., 2019; de Castro et al., 2020), forming hybrid (or mixed) depositional systems which are
53 represented in the stratigraphic record as unidirectionally migrating turbiditic channels (Gong et al.,
54 2013, 2018; Li et al., 2013), asymmetric turbiditic channels, laterally migrating levees (Carter and
55 Carter, 1988; Michels et al., 2002; Kuvaas et al., 2004; Sansom, 2018; Serra et al., 2020) that may
56 eventually evolve into mixed contourite drifts (Rebesco et al., 2002), and laterally elongated fans
57 (Fongnesu et al., 2020). Regional conditions may also favour the co-existence of turbiditic fans and
58 contouritic drifts (Locker and Laine, 1992; Faugères et al., 1999; Michels et al., 2002; Ercilla et al., 2016;
59 Juan et al., 2020). Another type of interaction is represented by turbidity systems reworked or even
60 eroded by subsequent bottom current intensification (Locker and Laine, 1992; Mulder et al., 2009;
61 Miramontes et al., 2019). In the opposite case, pre-existing contourite drifts may be dismantled by
62 mass movements that evolve distally into turbiditic deposits (e.g., Martorelli et al., 2016; Teixeira et
63 al., 2019). Finally, turbidites (or more generally, the products of mass flows) may alternate along time
64 with contourites in the long term, where turbiditic products are progressively substituted by
65 contourite drifts (Locker and Laine, 1992; Rasmussen et al., 2003), or driven by glacial-interglacial sea-
66 level cyclicity, leading to high-frequency turbiditic-contouritic sequences (Mulder et al., 2009).

67 The Gulf of Cadiz hosts an extensive contourite depositional system, particularly documented along
68 the Iberian margin, where the action of bottom currents over a complex, irregular seafloor topography
69 has generated different morpho-sedimentary erosive and depositional sectors (Hernández-Molina et
70 al., 2003, 2006; Llave et al., 2007a,b). Interactions between a number of gravity-driven and bottom
71 current-related processes are common in the Gulf of Cadiz, such as: the development of gravitational
72 erosive valleys that were later reoccupied by MOW filaments in the middle slope (Hanquiez et al.,

73 2010); long-term to short-term alternations between downslope mass wasting/turbidite systems and
74 along-slope contourite systems (Brackenridge et al., 2013; Alonso et al., 2016; García et al., 2016; de
75 Castro et al., 2020); deviation of the main MOW flow by submarine canyons and differential
76 development of contourite drifts (Mulder et al., 2006; Marchès et al., 2007) and high-frequency
77 turbidite-contourite variability in a slope terrace located between two submarine canyons (Marchès et
78 al., 2010) south of Portugal.

79 In the Gulf of Cadiz continental slope close to the Strait of Gibraltar, interactions between
80 contouritic and gravity-driven processes have not been fully appreciated. However, this area is ideal
81 for studying such kind of interactions, due to the occurrence of several outcropping and buried diapiric
82 bodies and ridges (Fernández-Puga et al., 2007), and their associated tectonic deformation (León et al.,
83 2010). The obstacle effect caused by the diapiric structures may influence bottom currents, generating
84 a suite of contourite depositional and erosional morphologies such as contourite channels and
85 sediment drifts (Palomino et al., 2016; Schattner et al., 2018). In addition, oversteepening due to
86 halokinetic processes and their associated overburden and faulting may favour the occurrence of slope
87 instabilities and associated mass movements (Cashman and Popenoe, 1985; Tripsanas et al., 2003,
88 2004; Akinci and Sawyer, 2016; Maselli and Kneller, 2018).

89 The interactions between the MOW and the middle slope erosive and depositional features have
90 been extensively studied and increased effort is invested in investigating the present-day influence of
91 the oceanographic dynamics with sedimentary processes at the seafloor (Lozano et al., 2020).
92 However glacio-eustatic cyclicity has been demonstrated to induce important changes in the spatial
93 distribution of water masses along glacial cycles (Llave et al., 2001, 2006, 2007a,b, Toucanne et al.,
94 2007; Marchès et al., 2010; Roque et al., 2012), suggesting that present-day morphology may result
95 from oceanographic patterns that were significantly different from the current ones. Considering the
96 existing knowledge gaps in understanding the evolution of this part of the margin, this study aims to
97 understand how the interactions between tectonic, sedimentary and oceanographic processes have
98 controlled the evolution of the continental slope in the vicinity of the Strait of Gibraltar. For this
99 purpose, the study area extends from the upper slope to the proximal middle slope of the northern
100 Gulf of Cadiz to a maximum water depth of about 600 m (36°10'-36°40'N, 6°30'-7°W). In particular,
101 this work aims at investigating the interactions between the diapiric structures and their associated
102 tectonic deformation and the climatically controlled gravitational and contouritic processes since the
103 middle Pleistocene.

104 **2. Geological and oceanographic framework**

105 *2.1. Geological setting*

106 The Gulf of Cadiz is located at the Atlantic side of the Strait of Gibraltar, limited to the north by the
107 SW Iberian Peninsula and to the south by NW Africa (Fig. 1a). The present-day geological setting is the
108 result of a complex tectonic history, after the opening of the Neo-Tethys and Central Atlantic in the
109 Triassic (Terrinha et al., 2002; Medialdea et al., 2009), and a series of tectonic phases related to the
110 movements along the African-Eurasian plate boundary (Rosenbaum et al., 2002). Half-graben and
111 horst structures produced by Mesozoic extension were reactivated as dextral strike slip faults during
112 Cenozoic compressional events (Lopes et al., 2006). During the Burdigalian-Middle Tortonian, the
113 westward drift of the Alboran Crustal Domain generated the Betic-Rifean thrust belt during a
114 compressive phase that reactivated NNW-SSE to NW-SE structures (Rosenbaum et al., 2002; Platt et
115 al., 2003, 2013). As a result, the Allochthonous Unit of the Gulf of Cadiz (AUGC) was emplaced during
116 the Late Tortonian (Torelli et al., 1997; Maldonado et al., 1999; Somoza et al., 1999; Medialdea et al.,
117 2004, 2009; Gütscher et al., 2009, 2012) and was reactivated in the Late Miocene to Present due to
118 NW compression. Salt diapirism rooted in Triassic evaporites and Miocene clay and marl diapirism
119 related to the AUGC (Medialdea et al., 2009) have produced widespread NE-SW-oriented diapiric
120 ridges (Cadiz, Guadalquivir and Doñana diapiric ridges, Fig. 1) that have been reactivated during the
121 Pliocene–Quaternary as the result of adjustments in the allochthonous unit under a dominant NW-SE
122 compressive regime (García et al., 2009; Fernández-Puga et al., 2010; Hernandez-Molina et al., 2016).
123 Major structures in the Gulf of Cadiz (thrust faults, strike-slip faults, extensional faults and diapirs)
124 favour the upward fluid escape that originate minor features as mud volcanoes and pockmarks (Casas
125 et al., 2003; Somoza et al., 2003; Fernández-Puga et al., 2007).

126 *2.2. Oceanographic setting*

127 The present-day oceanographic setting of the Gulf of Cadiz is dominated by the water exchange
128 between the Mediterranean Sea and the Atlantic Ocean, through the Strait of Gibraltar (Figs. 1a and
129 2). At the western side of the strait, the water column along the Gulf of Cadiz continental margin is
130 occupied by distinct water masses. The inner shelf waters reach depths down to 60 m, impinging
131 directly on the continental shelf and are subject to coastal and atmospheric influence (Bellanco and
132 Sánchez-Leal., 2016; Sánchez-Leal et al., 2017). The low-salinity Eastern North Atlantic Central Water
133 (ENACW) circulates with the same direction but at depths of 100-250 m, affecting the outer
134 continental shelf and the shallower upper slope. Below, the Mediterranean Outflow Water (MOW)
135 circulates towards the NW (Fig. 2b; Sánchez-Leal et al., 2017) sweeping most of the upper slope and
136 the middle slope. The MOW, after exiting the Strait of Gibraltar at depths deeper than 150-200 m
137 veers towards the NW, where it is affected by the interaction with the rough topography (Fig. 2a;
138 Sánchez-Leal et al., 2017). Its upper boundary deepens as it flows north-westwards along the Gulf of
139 Cadiz continental margin and it is split into two preferential pathways forming the Mediterranean

140 Upper Core (MU), that flows along the base of the upper slope, and the Mediterranean Lower Core
141 (ML), flowing along the middle slope (Fig. 1a; Madelain, 1970; Zenk, 1975; Grundlingh, 1981; Borenäs
142 et al., 2002; Serra et al., 2005, 2010; Sánchez-Leal et al., 2017). The modified Antarctic Intermediate
143 Water (AAIW) also flows towards the NW, down to depths of 600-625 m, and confines the MOW and
144 the ENACW against the continental slope (Louarn and Morin, 2011; Hernandez-Molina et al., 2014;
145 Roque et al., 2019). Finally, the North Atlantic Deep Water (NADW) flows below the MOW towards the
146 E-SE at water depths >1500 m (Zenk, 1975; Thorpe, 1976; Gardner and Kidd, 1983; Ochoa and Bray,
147 1991; Baringer and Price, 1999; Serra et al., 2005).

148 The oceanographic pattern in the Gulf of Cadiz is highly dynamic and exhibits drastic seasonal
149 changes. During the month of March, cooler and less saline waters (temperature of 14.6°C and
150 practical salinity of 36.26) occupy the inner shelf due to the erosion of the seasonal thermocline and
151 the increase in river water supply and denser MOW (colder and more saline) invades the upper slope,
152 displacing the ENACW towards the shelf. In November conditions, the water stratification is intensified
153 and the ENACW broadens and stretches eastwards (Bellanco and Sánchez-Leal, 2016). In addition, a
154 displacement of the MOW toward the upper continental slope is further favored by the increased
155 presence of AAIW and a reduction of the ENACW (Roque et al., 2019).

156 *2.3. The Gulf of Cadiz Contourite Depositional System*

157 The Gulf of Cadiz hosts a huge contourite depositional system (CDS), created by the MOW as it exits
158 the Strait of Gibraltar into the Atlantic Ocean. This system has been extensively studied in the last
159 decades (Gonthier et al., 1984; Nelson et al., 1993, 1999; Maldonado et al., 1999; Llave et al., 2001,
160 2007; Hernández-Molina et al., 2003, 2016; Roque et al., 2012), mostly focusing on the erosional and
161 depositional features in the middle slope (Fig. 1a; Hernández-Molina et al., 2006). The study area lies
162 in the limit between the proximal scour and sand ribbons sector, close to the Strait of Gibraltar, and
163 the active contourite drift sector towards the NW (1 and 2 respectively in Fig. 1a). The proximal sector
164 presents two channel-terrace systems, Northern and Southern, that connect with the middle slope
165 contourite channels (Hernández-Molina et al., 2014). The active contourite drift sector contains the
166 Faro-Cadiz sheeted drift that evolves towards the west into huge mounded drifts (e.g., Faro Drift)
167 separated from the upper slope by the Alvares Cabral contouritic moat (Fig. 1a).

168 After the Miocene-Pliocene boundary, the Strait of Gibraltar became the gateway for the MOW
169 into the Atlantic and the CDS recorded a series of tectonic pulses of different cyclicity that defined
170 three evolutionary stages (Hernández-Molina et al., 2016): (1) Initial-drift stage (Pliocene, 5.33-3.2
171 Ma). Sedimentation was dominated by downslope processes, mostly turbiditic and debris flows while
172 the progressive strengthening of a relatively weak MOW deposited large muddy sheeted drifts; (2)

173 Transitional drift stage (late Pliocene-early Quaternary, 3.2-2 Ma). This stage was characterized by
174 interbedded contourites and turbidites, and occasional debrites, indicating a progressive
175 intensification of the MOW strength; and (3) Growth-drift stage (after 2 Ma). Bottom-current activity
176 prevailed over downslope-trending processes and shaped the present-day Gulf of Cadiz Contourite
177 Depositional System (Hernández-Molina et al., 2016). This last Quaternary stage includes three main
178 phases (Llave et al., 2001, 2006, 2007a,b, 2011). From the Early Pleistocene to the Mid-Pleistocene the
179 MU core flowed along the base of the upper slope and mounded and sheeted drifts were deposited on
180 the upper-middle slope boundary. Between the Mid Pleistocene and the Late Pleistocene, the MU core
181 migrated northward due to changes in the tectonic activity of the Guadalquivir Bank and the diapiric
182 ridges. During this stage, the main MOW flow that was previously conducted through five channels at
183 the exit of the Strait of Gibraltar migrated to its present-day location along the Southern channel (Llave
184 et al., 2019). These oceanographic changes resulted in the formation of mixed drifts, involving
185 interaction between bottom current activity and gravitational processes that buried part of the
186 sheeted and mounded drifts. During the Late Pleistocene to Holocene, a further northward migration
187 of the MU core, that flowed with a more tabular character connecting with the Northern channel,
188 resulted from tectonic movements in the Strait of Gibraltar and the reactivation of diapiric bodies,
189 while the Southern Channel maintained its present-day position (Llave et al., 2019). During this stage
190 the Gusano and Huelva channels were excavated on the proximal middle slope, and the mixed drifts
191 were fossilized by a more aggrading plastered drift at the transition between the upper and middle
192 slope. In this scenario, the MU core flow along the upper slope and upper terrace was favoured during
193 warm highstand intervals, whereas the Lower core flow predominated along the middle slope, or even
194 in deeper depths, during cold lowstand intervals (Llave et al., 2007a,b; Hernández-Molina et al., 2014;
195 Lofi et al., 2016).

196 *2.4. The Gulf of Cadiz upper slope*

197 The upper slope along the Gulf of Cadiz has only been partially studied so far. The SE part of the
198 northern Gulf of Cadiz upper slope is dominated by plastered contourite drifts incised by erosive
199 scarps (Nelson et al., 1993, 1999; Llave et al., 2007b; Hernández-Molina et al., 2014; Brackenridge et
200 al., 2018). The plastered drift along the Cadiz upper slope is composed of highly bioturbated silts to
201 sandy silts and displays characteristic bi-gradational sequences (Brackenridge et al., 2018), and results
202 from the interplay of bottom currents and turbidity currents/spillover processes as the main sediment
203 supply (Nelson et al., 1993, 1999; Hernández-Molina et al., 2014; Alonso et al., 2016). The upper slope
204 in this area is incised by numerous gullies that have been studied from a geostatistical point of view
205 and related to gravitational flows since the Last Glacial Maximum, fed from the Guadalquivir and
206 Guadalete rivers and mass wasting sediment supply (Fernández-Salas et al., 2015; Sánchez-Rubio et al.,

207 2015). Deposits belonging to regressive and lowstand systems tracts and accumulated during the Late
208 Quaternary compose the middle to lower slope sequences (Rodero et al., 1999; Mestdagh et al., 2019,
209 2020). Towards the NW, the upper slope becomes the erosional northern wall of the Alvares Cabral
210 contourite moat (Faugères et al., 1984; Llave et al., 2001; García et al., 2009; Roque et al., 2012; Fig.
211 1a). The westernmost upper slope, in the Portuguese margin, is dominated by the interplay between
212 contouritic and turbiditic processes, with the incision of the Portimão, Lagos and Sagres submarine
213 canyons in the contourite-dominated middle slope and down to the deeper basin (Mulder et al., 2006;
214 Marchès et al., 2007, 2010; Fig. 1a).

215 **3. Datasets, methodology and nomenclature**

216 *3.1. Datasets and methodology*

217 This work analyses geophysical and geological datasets with different degrees of resolution (Fig.
218 1b). The regional bathymetry has a resolution of 500 m and has been obtained from the GMRT Map
219 Tool (Ryan et al., 2009). The study area is covered with a high-resolution swath bathymetry data
220 compiled along a series of cruises (SWIM compilation, Diez et al., 2005; CONTOURIBER, MOWER,
221 INDEMARES) and gridded at a resolution of 50 m. Visualization and interpretation of bathymetric data
222 were achieved using Fledermaus, Global Mapper and Mirone softwares. Airgun profiles were acquired
223 during the CONTOURIBER and MOWER cruises. They are oriented NNW-SSE and WNW-ESE. Airgun 2-D
224 seismic reflection profiles were acquired using different arrangements of 610-910 cu.in GI-airguns
225 adapted to the water depth and quality of the signal. Shot frequency was 6 seconds and sampling rate
226 of 0.5 ms. During the cruises navigation was controlled by the EIVA NaviPac and the vessel was
227 positioned with a GPS dynamic system. The data were acquired with a three-channel (40
228 receivers/channel), 250 m long SIG streamer and recorded with a DELPH system. The vertical
229 resolution of the seismic profiles is less than 10 m. Processing was performed with the Hotshots
230 software and followed standard procedure, including equalization, low frequency filtering, band-pass
231 filtering, stacking, and resampling to 1 ms. A grid of NE-SW and NW-SE-oriented multichannel 2-D
232 seismic reflection profiles were provided by Repsol-YPF (S81). The entire seismic data set has been
233 visualized and interpreted using the Kingdom Suite software.

234 High-resolution data (bathymetry and seismic profiles) have been analyzed in order to characterize
235 the morphological features. To study the late Quaternary evolution of the upper slope, airgun seismic
236 profiles have been correlated with previous regional stratigraphic studies based on the analysis of
237 multichannel 2-D seismic reflection profiles (Hernández-Molina et al., 2016; Figs. 1b and 3). Two major
238 unconformities (Mid Pleistocene Discontinuity, MPD and Late Quaternary Discontinuity, LQD) were
239 identified after the Integrated Ocean Drilling Program (IODP) Expedition 339 and with the additional

240 information from well MPC-1 located in the upper slope of the studied area (Hernández-Molina et al.,
241 2016). Despite the different resolution, these horizons can be translated to the dataset used in this
242 study (Fig. 3). The seismic units correspond to the most recent Quaternary units (QIII) identified by
243 Hernández-Molina et al. (2016) and QII (Llave et al., 2001, 2007, 2011; Brackenridge et al., 2013). The
244 MPD has also been interpreted in previous studies (Fig. 3) as the Mid Pleistocene Revolution
245 discontinuity (Llave et al., 2001, 2007, 2011; Hernández-Molina et al., 2003, 2006; Brackenridge et al.,
246 2013), D2 (Marchès et al., 2010) or H4 (Roque et al., 2012). The discontinuity bounding units Q5 and
247 Q6 correlates with discontinuities LQD (Hernández-Molina et al., 2016), D3 (Marchès et al., 2010) and
248 H5 (Roque et al., 2012). The analysis of multichannel seismic profiles has allowed controlling the slope
249 sedimentary evolution, and to analyze the structural features affecting the sediment record. The
250 analysis of high-resolution seismic profiles (airgun) has allowed a more detailed characterization of the
251 geometry, distribution and character of the seismic units in a temporal scale from the Middle
252 Pleistocene to present. The penetration of these profiles and the presence of the bottom multiple
253 reflection only allows a detailed description of the most recent unit, Q6. In addition, the multichannel
254 seismic profiles have been used to obtain isochore maps of the seismic units identified in this work.

255 3.2. Nomenclature

256 Morphological features are identified based on their morphometric parameters, spatial distribution
257 and seismic characteristics. Contouritic morphological features (contourite drifts, channels, furrows,
258 terraces) follow the nomenclature established by Faugères et al. (1993a,b, 1999), García et al. (2009)
259 and summarized by Rebesco et al. (2014). Sediment waves are identified based on the bathymetry and
260 on their internal geometry observed in seismic profiles, with changes in the thickness of individual
261 seismic layers (Berndt et al., 2006; Viana, 2009). Mass transport deposits (MTDs) are defined based on
262 their seismic signature including a basal erosional surface, top hummocky relief at the top and internal
263 chaotic to transparent seismic facies (Shanmugam, 2007; Posamentier and Martinsen, 2010;
264 Shanmugam, 2012; Ruano et al., 2014). Mass movement erosional features include submarine valleys
265 and escarpments. Upper slope valleys are classified as gullies, based on their downslope trend (Fedele
266 and Garcia, 2009), and their dimensions -an order of magnitude smaller than submarine canyons (Field
267 et al., 1999; Rinke-Hardekopft et al., 2018). Shelf-edge escarpments are interpreted as slide scars
268 based on their arcuate-linear shape and their step-like profiles that truncate underlying seismic
269 reflections (Mulder and Cochonat, 1996; McAdoo et al., 2000; Twichell et al., 2009; Piper et al., 2012;
270 García et al., 2016). Fluid-escape features are defined by their circular- to elliptical plan-view shape in
271 the seafloor (Hovland and Judd, 1988; Schattner et al., 2018), their characteristic seismic signature
272 (Cartwright and Santamarina, 2015) and based on previous descriptions (Baraza and Ercilla, 1996;
273 Baraza et al., 1999; León et al., 2010).

274 4. Results

275 4.1. Physiography and morphology

276 4.1.1. Physiography

277 The continental margin close to the Strait of Gibraltar extends for about 100 km with a SSE-NNW-
278 orientation, turning to a ESE-WNW orientation off the Guadalquivir river mouth (Figs. 1a and 4a). The
279 continental shelf-edge in this proximal part of the margin is relatively smooth along the study area and
280 occurs at water depths of 110-130 m. The upper slope reaches depths of 390-480 m, extending deeper
281 in the area off Cadiz, to the east of the Cadiz diapiric ridge (green profiles in Fig. 4b). The upper slope
282 profile is flat to convex-upward in the south and central part of the study area and flat to concave-
283 upwards in the north (Fig. 4b). A marked change in the slope gradient marks the transition between
284 upper and middle slope except for the central part of the study area, where the transition is smooth
285 and bulge-shaped (Fig. 4b).

286 In the studied sector (Figs. 4 and 5) the physiography of the upper and middle slope allows the
287 establishment of three areas with distinct bathymetric profiles: Southern, Central and Northern (Fig.
288 4a). The Southern area displays a featureless upper slope with a convex-upwards profile and widths of
289 about 16 km (Fig. 4b). Its lower limit, at about 500 mwd, connects with a narrow and steep ramp (2 km
290 wide and 3° slope gradient) that connects with the Northern contourite channel in the middle slope.
291 The channel is incised at the western part of a 35 km wide terraced platform at 670-770 mwd that
292 limits towards the NW with the Cadiz and Huelva contourite channels (Fig. 4a). The Central area shows
293 a relatively flat upper slope profile, with width increasing towards the north from about 5 km to a
294 maximum of 22 km, whereas the steepness decreases from about 3° to 1.2° (Fig. 4b). The connection
295 with the Northern channel in the middle slope occurs at water depths of about 500 m through a steep
296 ramp (< 1 km wide and up to 7°) (Fig. 4b). The Northern area has a convex-upward upper slope with a
297 width that decreases towards the north to about 12 km, and the steepness ranges between 1 and 2.2°
298 (Fig. 4b). It connects smoothly with the middle slope at water depths of 400-450 m. The middle slope
299 has a lower gradient (less than 0.7°) and connects with the Faro-Cadiz sheeted drift at the eastern side
300 of the Cadiz diapiric ridge. The sheeted drift is bounded towards the west by the Tofiño contourite
301 channel and the Cadiz diapiric ridge and to the south by the Huelva contourite channel (Fig. 4b).

302 4.1.2. Morphological features

303 A range of morphological features have been identified in the study area, and are classified
304 according to their origin as (i) structural, including the diapiric highs and ridges, (ii) contouritic,

305 represented by a large plastered drift, sediment waves and contourite channels, (iii) gravitational,
306 including escarpments and gullies, and (iv) fluid-escape related features.

307 (i) Structural features. The Cadiz diapiric ridge (CDR; Figs. 4a and 5b) is the main outcropping
308 diapiric feature in the study area. The ridge has an N-S to NNE-SSW orientation. Its northern part
309 outcrops in the middle slope close to the limit with the upper slope in the Northern area and is
310 dissected by the Gusano and Tofiño contourite channels. The southern part lies between the Huelva
311 and Cadiz contourite channels. The ridge has isolated peaks up to about 200 m in height, with a
312 minimum water depth of 320 m.

313 (ii) Morphological features of contouritic origin. The *plastered drift* that makes up the upper slope
314 (Hernández-Molina et al., 2014; Brakenridge et al., 2018) has a typical convex-upwards morphology,
315 and the rest of morphological features are overprinted on its relatively flat surface (Fig. 4). *Sediment*
316 *waves* are superimposed on the plastered drift in the Northern area. They are oriented SE-NW to S-N
317 (parallel to slightly oblique to the isobaths; Fig. 5c). Individual crests are around 0.5-1 km long, and the
318 wavelength averages 0.5 km. Sediment waves are asymmetric, with steeper downslope-facing flanks
319 (up to 2.4°) and almost flat upslope-facing flanks. *Contourite channels* (Northern, Southern, Cadiz,
320 Huelva, Gusano and Tofiño) are major erosional features composing the Gulf of Cadiz Contourite
321 depositional system (Hernández-Molina et al., 2003; García et al., 2009; Lozano et al., 2020). The upper
322 slope connects with the Northern channel defined by Hernández-Molina et al. (2014) at 530-580 mwd
323 in the Southern and Central areas (Fig. 5b). The Northern channel joins the Huelva and Cadiz
324 contourite channels along the distal limit of the upper slope and is absent in the Northern area of this
325 study (Fig. 4a).

326 (iii) Gravitational features. *Shelf-edge escarpments* occur in the Central and Northern areas (Figs. 5b
327 and 5d). A prominent arcuate escarpment at the shelf-edge of the Central area is 20 m high and about
328 4 km long. Basinwards of the escarpment the bathymetric profile is concave-upwards (Fig. 5d). Linear,
329 up to 8 m high N-S to NW-SE-oriented escarpments occur along the shelf-edge of the Northern area. A
330 12 km long linear escarpment 30 m deep and 5° steep occurs in the Southern area at the limit with the
331 Northern channel, where the channel trend changes from SSE-NNW to SE-NW (Fig. 5b). *Gullies* occur
332 on the Central and Northern areas (Fig. 5b) Gullies in the Central area extend from 205-250 mwd,
333 below the continental shelf-edge, to the rim of the Northern channel. Gullies are generally
334 asymmetric, with steeper and higher NW walls and present V-shaped profiles (Fig. 5e), 12-20 km long,
335 2-25 m deep and 0.2-1 km wide. Their orientations range ENE-WSW to NE-SW, they are spaced 0.4-2
336 km and display a dendritic convergent pattern (Fig. 5b). Gullies are less common in the Northern area.
337 Their heads are located at 205-240 m, and they terminate at water depths of 405-415 m, in the

338 relatively flat Faro-Cadiz sheeted drift on the middle slope (Fig. 5b). They are smaller (5.5-9.5 km long;
339 0.2-0.4 km wide and 1-3 m deep) than in the Central area and have asymmetric U- or V-shaped profiles
340 (Fig. 5e). They are E-W to ENE-WSW-oriented, with linear trends and they occur as individual features,
341 spaced 0.3-1 km.

342 (iv) Fluid-escape features are circular- to elliptical-shaped depressions identified in the deeper part
343 of the upper slope in the Central area close to the rim of the Northern channel (Fig. 5b). They are up to
344 1.5 km wide and 70 m deep. Most of them are aligned along the axes of gullies and their long axis have
345 similar orientations (roughly NNE-SSW) whereas others occur in inter-gullies areas and are oriented
346 parallel to the bathymetric contours.

347 4.2. Seismic analysis

348 4.2.1. Acoustic basement and structural features

349 The topography of the acoustic basement in the study area is highly irregular, with depths ranging
350 between 0.5 and 3.7 s two-way travel time (TWTT; Fig. 6a). A prominent acoustic basement high in the
351 SE part of the study area delimits a NE-SW-trending depression extending from the present-day
352 continental shelf to the middle slope. Basement highs coincident with the Cadiz and Guadalquivir
353 diapiric ridges delimit a second NE-SW oriented basement depression that opens towards the SW.
354 Other minor basement highs roughly coincide with the present-day shelf-edge, whereas most of the
355 upper slope is characterized by basement highs delimiting irregular depressions.

356 Diapir tops are spatially associated to the basement topography (Fig. 6a). Apart from the
357 outcropping diapiric ridges, most diapirs are buried and their tops are aligned with two predominant
358 orientations: NE-SW and NW-SE. The top of most of the upper slope buried diapirs as well as the two
359 outcropping diapiric ridges are oriented NE-SW to ENE-WSW. Below the distal limit of the Central area
360 a NE-SW diapir and its associated faults reach the seafloor. Columnar zones of acoustic amplitude
361 anomalies and truncated seismic reflections connect vertically with the circular- to elliptical-shaped
362 fluid-escape depressions on the present-day sea-floor and in the seismic record (Figs. 5b, 7b and 8b).
363 Some other diapirs are aligned in a perpendicular NW-SE to WNW-ESE direction (Fig. 6a). They occur in
364 the present-day Cadiz contourite channel, in the upper slope of the Central area (where the heads of
365 many gullies occur), on the upper slope at the limit between the Northern and Central areas
366 (coinciding with the distal end of many gullies), and at the NW side of the outcropping Cadiz diapiric
367 ridge, where the Gusano channel is excavated. Faults are widespread features in the sedimentary
368 record of the Cadiz upper slope (Figs. 6b to 10). They are mostly normal faults that are rooted in the
369 diapirs, both at their tops and flanks and can be defined as extensional crestal faults (Jackson and

370 Hudec, 2017). Faults rarely reach the seafloor, and are often associated to the gullies and to the fluid-
371 escape features (Figs. 6b to 10).

372 4.2.2. Seismic stratigraphy

373 The two major seismic discontinuities (MPD- Mid Pleistocene Discontinuity and LQD- Late
374 Quaternary Discontinuity) define two major late Quaternary units, following the most recent regional
375 nomenclature proposed by Hernández-Molina et al. (2016) (Figs. 3c and 3d): a) Seismic Unit Q5 (MPD-
376 LQD, subdivided into three sub-units, Q5-a to Q5-c) and b) Unit Q6 (LQD-Present, composed of four
377 sub-units, Q6-a to Q6-d). All discontinuities are better defined in the proximal upper slope by
378 pronounced changes in the frequency and acoustic amplitude of reflections. The character of units and
379 sub-units and the main seismic features are shown in Figures 7 to 11. The topography of the basal
380 discontinuities bounding each unit and their thickness distribution are shown in Figure 12.

381 a) Seismic Unit Q5: MPD-LQD

382 The seismic configuration of Q5 unit shows a mostly aggrading stacking pattern with parallel
383 stratified reflections of medium to high amplitude and interlayered wavy-chaotic packages with
384 disrupted reflections, in the Southern area (Figs. 7 to 9). The Central area shows layered and wavy-
385 chaotic disrupted reflections that display a progradational configuration towards a paleo-channel
386 about 6 km to the east of the present-day Northern channel (Fig. 10). In the Northern area, Q5 mostly
387 presents parallel stratified reflections. V- or U-shaped erosional depressions are mostly identified in
388 the seismic lines parallel to the bathymetric contours and occur mostly associated to diapir-related
389 faults. They are more common in the top of the unit where they occur around diapiric highs in the
390 Southern area and show vertical migration towards the NW (Fig. 8a). Q5 is deformed by the NE-SW
391 and the NW-SE trending diapiric alignments and related faults, with upward tilting and thinning
392 towards the diapiric highs (Figs. 7 to 11).

393 The overall distribution of Q5 is patchy, with depocenters up to 360 ms TWTT thick located
394 between diapir highs and pronounced decreases in thickness towards the top of isolated diapiric
395 diapiric ridges (Fig. 12a). Depocenters are smaller in the Northern area, whereas the Central and
396 Southern areas contain wider and thicker depocenters (230-360 ms TWTT) on the present-day shelf-
397 edge and upper slope. The geometry of the seismic unit Q5 is tabular in the Southern and Central
398 areas (Figs. 9 and 10). In the Central area, thickness decreases in a paleo-channel displaced about 6 km
399 to the east of the present-day Northern channel. In the Northern area (Fig. 11), the geometry ranges
400 from wedge-shaped, with higher thickness towards the proximal areas of the slope to lens-shaped,
401 with minimum thickness towards the flanks of diapiric bodies. During deposition of Q5 the topography

402 of the upper slope changed significantly (MPD base surface to LQD base surface; Fig. 12b to 12d)
403 producing: a) the infilling of the NE-SW-trending depressions at the SE of the study area and between
404 CDR and GDR; b) the infilling of small depressions at the present-day base of the upper slope; c) the
405 advance of the continental shelf-edge to positions similar to the present-day.

406 Three sub-units compose the seismic unit Q5 (Q5-a, Q5-b and Q5-c, from older to younger). The
407 three sub-units have similar distribution patterns, with a progressive displacement of depocenters
408 towards the present-day shelf-edge (Figs. 7 to 11). Q5-a (MPD-5b discontinuities) has mid to high
409 acoustic amplitude in generally parallel layered reflections. It displays maximum thickness in the
410 present-day shallower upper slope of the Central and Northern areas, and in the middle upper slope of
411 the Northern area. Q5-b (5b-5c discontinuities) has lower acoustic amplitude than Q5-a and its
412 depocenters are aligned along the present-day shallower upper slope of the Southern and Central
413 areas. Q5-c (5c-LQD discontinuities) is characterized by low-acoustic amplitude at the base that
414 become higher towards the top. Its thickness is higher along the shallower upper slope of the Central
415 area, and on the middle upper slope of the Southern area.

416 b) Seismic Unit Q6: LQD-seafloor

417 The seismic configuration of Q6 shows layered reflectors locally interbedded with packages of
418 disrupted reflections in the Central and Northern areas, and lower acoustic amplitude than Q6 (Figs. 7
419 to 11). Q6 is widely deformed by NW-SE buried diapir alignments and the outcropping diapiric ridges,
420 but deformation by NE-SW-oriented ones is drastically diminished. The NW-SE-oriented diapir
421 alignment located in the limit between the Central and Northern areas only deforms Q6, whereas the
422 underlying unit Q5 is not affected. Seismic unit Q6 is much less deformed by diapir-related faults than
423 Q5, in particular towards the top (Figs. 7 to 11).

424 The overall distribution of Q6 is different from the underlying Q5, showing greater thickness (up to
425 660 ms TWTT) and a more homogeneous distribution (Fig. 12c). The main depocenter locates below
426 the present-day shelf edge, at the limit between the Northern and Central areas. Thickness decreases
427 towards the CDR and GDR and the buried NW-SE-oriented diapiric alignments at the eastern side of
428 the CDR. The deposition of Q6 resulted in the growth of the present-day upper slope to the NE rim of
429 the Northern contourite channel, that presents minimum thicknesses (<200 ms TWTT). Since the LQD,
430 the main changes in the topography include the infilling of previous depressions, the excavation of the
431 Gusano contourite channel to the north of the CDR and the incision of gullies (Fig. 12d).

432 Q6 is composed of four sub-units (Q6-a to Q6-d, from older to younger). Whereas the four sub-
433 units show a similar pattern of deformation, their distribution, geometry and internal configuration
434 have important differences and will be described individually.

435 Q6-a sub-unit (LQD – 6b discontinuity) has a tabular geometry with layered reflections in the
436 Southern area. The unit displays increased thickness and disrupted reflections in the footwall side
437 (basinward) of a set of diapir-related faults (Fig9 8). It displays maximum thickness of about 0.12 s
438 TWTT in the Central area upper slope at the footwall side of a set of diapir-related faults. Thickness is
439 significantly low in the shallower upper slope and particularly at the proximal middle slope, at the
440 eastern side of a paleo-channel, slightly displaced to the west of the present-day Northern channel
441 (Fig. 10). V- and U-shaped depressions occur both within the sub-unit and incised in the top
442 discontinuity, generally associated to faults (Figs. 7b and 8a). Towards the Northern area, Q6-a shows
443 layered reflections with V-and U-shaped depressions in the deeper areas between diapirs, and the
444 thickness is generally low (Figs. 7 and 8). This sub-unit is generally thin with maximum thickness of
445 about 180 ms TWTT in a wide depocenter on the deeper part of the present-day upper slope.

446 Q6-b (6b-6c discontinuities). This sub-unit displays similar seismic characteristics as Q6-a in the
447 Southern area, but the depocenter is slightly displaced upslope (Fig. 9). In the Central area the upslope
448 displacement of the deposition is more evident as well as a thickness decrease below the present-day
449 Northern channel (Fig. 10). In the Northern area the base of the sub-unit has a transparent to chaotic
450 character with disrupted reflections (Figs. 7 and 11). The sub-unit presents numerous small V-shaped
451 depressions in the deepest part of the upper slope and thickness increases significantly between
452 diapiric highs.

453 Q6-c (6c-6d discontinuities). This sub-unit is mostly layered in the entire study area. The top
454 boundary shows erosional truncations in the Southern area. It presents few V- or U-shaped
455 depressions in the Central area, in most cases associated with faults (Figs. 7 and 10). In this area, Q6-c
456 displays mounded configurations with upslope progradation on the deeper part of the upper slope, at
457 the foot wall of a set of diapir-related faults (detail in Fig. 10). In the Northern area V- and U-shaped
458 depressions only occur at the top boundary (Fig. 11). Q6-c is relatively thin, particularly in the Southern
459 area. Maximum thickness (around 0.2 s TWTT) occur in the Central area where the distribution is
460 affected by the diapiric highs. The Northern area shows depocenters in the depressions between
461 diapiric highs.

462 Q6-d (6d discontinuity- seafloor) displays a stratified character with very low acoustic amplitudes in
463 in the Southern and Central areas (Figs. 9 and 10). In the Central area layered reflections are cut by V-
464 shaped depressions along the entire sub-unit that show a NW upward migration (Fig. 8). Q6-d displays

465 a distinctive wavy-chaotic seismic character with disrupted reflections at the shallower upper slope in
466 the Northern area and chaotic-transparent in the deeper parts where it connects with the middle
467 slope (Fig. 11). The main depocenters occur at shallower depths than the previous sub-units, along the
468 present-day shelf-edge in the Central area.

469 5. Discussion

470 The physiographic, morphologic and seismic stratigraphic analysis presented in the previous sections
471 allow inferring the sedimentary processes that have shaped the upper slope and proximal middle slope
472 of the Gulf of Cadiz in the study area and to analyze their evolution since the MPD based in
473 chronostratigraphic correlations. Two major factors (sea-level changes and episodic tectonic activity)
474 are proposed to have controlled the sedimentary evolution of this part of the margin.

475 5.1. Sedimentary interpretation and chronostratigraphic correlations

476 Based on the results of this work and on previous published literature (Nelson et al., 1993, 1999; Llave
477 et al., 2007b; Hernández-Molina et al., 2014; Brackenridge et al., 2018; Mestdagh et al., 2020), the
478 upper slope is characterized by plastered drift deposition since the MPD, as suggested by the parallel-
479 stratified seismic character of high lateral continuity, aggrading pattern and tabular to slightly
480 mounded geometry (Faugères et al., 1999; Hernández-Molina et al., 2006; Van Rooij et al., 2010). At
481 the connection with the middle slope, the plastered drift limits with the Northern channel (Hernández-
482 Molina et al., 2014) that can be defined as a contourite channel based on the along-slope trend and
483 the presence of truncated reflections (Figs. 4, 5 and 9 to 11; Faugères et al., 1999).

484 The LQD marks a change in the stacking pattern as the plastered drift-contourite channel system
485 migrated towards the SW, the plastered drift increased in thickness and the contourite paleo-channel
486 increased its incision in the proximal middle slope (Fig. 12). The chronostratigraphic correlation allows
487 interpreting the sedimentary evolution in relation with the two main discontinuities, the MPD and the
488 LQD. The MPD (base of seismic unit Q5) is a discontinuity that exhibits different stratigraphic character
489 in the Gulf of Cadiz continental slope, such as an erosive hiatus, a condensed section or a section with
490 reduced sedimentation rate in different locations, related to a tectonic event related with tectonic
491 shortening and gravitational spreading, with an age around 0.7–0.9 Ma (Hernández-Molina et al.,
492 2016; Lofi et al., 2016). It also corresponds to the Mid Pleistocene Revolution (MPR) in the quaternary
493 climatic discontinuity, related to the first important cold event and associated sea-level fall in the
494 Pleistocene (Llave et al., 2001, 2004; Hayward et al., 2005; Head and Gibbard, 2005; Ehlers and
495 Gibbard, 2007) and the MOW enhancement coeval with an increase in the sedimentation rates in the
496 Gulf of Cadiz (Llave et al., 2011; Roque et al., 2012; Hernández-Molina et al., 2016). LQD corresponds
497 to a hiatus in the time window of 0.3–0.6 Ma (Hernández-Molina et al., 2016; Lofi et al., 2016)

498 characterized in seismic profiles of the middle slope contourite drifts by an angular unconformity on
499 the basin margins and the flanks of the topographic highs that changes laterally to concordant
500 relationships in the middle of the basins (Hernández-Molina et al., 2016). This discontinuity has been
501 associated with a lowering of the sea level (Marchés et al., 2010) and an strengthening of the MOW
502 circulation in the middle continental slope (Roque et al., 2012).

503 *5.2. Influence of sea-level on sedimentation: paleoclimatic and paleoceanographic implications*

504 Sea-level change is a crucial factor controlling bottom current sedimentary processes (Rebesco et al.,
505 2014). The stacking pattern of the plastered drift and the adjacent Northern contourite channel allows
506 inferring the paleoclimatic and paleoceanographic conditions that influenced their evolution. The
507 results of this study suggest that the plastered drift grew under the activity of a weak ENACW flow,
508 whereas the contourite paleo-channel evolved by the erosive effect of the MOW, during regressive
509 and lowstand sea-level stages. Lowered sea-levels during glacial stages are characterized by enhanced
510 deep circulation that produces a more intense and deeper ML in the Gulf of Cadiz (e.g. Llave et al.,
511 2006, 2007, Toucanne et al., 2007; Marchès et al., 2010; Lofi et al., 2016) and even the probable
512 disappearance of the MU (Roque et al., 2012). Since the study area is located at the present-day
513 interface between the MOW and the ENACW (Fig. 2), the deepening of the MOW would have left the
514 entire upper slope under the effect of the ENACW during the lowstands of the asymmetric glacial
515 cycles. This scenario would last a longer period of time compared with the highstand situation in which
516 the MOW covers the upper slope, as at present. Furthermore, it is during sea-level lowstands that the
517 sediment supply from fluvial discharge and continental shelf, required to produce significant plastered
518 drift growth in this area is enhanced (Rodero et al., 1999; Mestdagh et al., 2019). Under this
519 assumption, sub-unit boundaries within Q5 and Q6 units can be tentatively linked to the 100 ky
520 Quaternary climatic oscillations as defined by the benthic $d^{18}O$ isotopic curve of Lisiecki and Raymo
521 (2005) (Fig. 3d).

522 V- and U-shaped depressions not related to diapir-associated faults are widespread along the seismic
523 sub-units (Fig. 3d) and we interpret them as paleo-gullies, based on the truncated reflections in their
524 flanks, the local presence of lateral deposits (levees) and their morphological resemblance with the
525 present-day gullies. Their occurrence supports that the bulk of the plastered drift growth affected by
526 gullies incision occurred during glacial climatic stages, assuming a genetic link between gully formation
527 and sea-level lowstands, as documented in other continental margins (Field et al., 1999; Spinelli and
528 Field, 2001). Gullies migration suggests southeastward bottom current activity, coincident with the
529 circulation pattern of the ENACW. Migrating trends upstream of the bottom currents have been
530 reported in modern sea-floor (Campbell and Mosher, 2016) and in the sedimentary record (Sansom,

531 2018; Fonnesu et al., 2020). Recent three-dimensional flume-tank experiments have explained how
532 low density turbidity flows can be deviated by weak along-slope currents and demonstrate that the
533 direction of migration of gravitational channels is opposite to the direction of the bottom current
534 interacting with them (Miramontes et al., 2020). Therefore, we propose that diffuse, sheet-like
535 turbidity currents presumably originating on the shelf as proposed by Lonergan et al. (2013) or
536 alternatively low density cascading water flows (Micallef and Mountjoy, 2011) were deflected by a
537 weak along slope current forming asymmetric gullies with their axes migrating up-current. During
538 transgressive and highstand stages the study area is, in contrast, under the influence of the MOW
539 (Sánchez-Leal et al., 2017). In these conditions, such as present-day, the plastered drift is reworked by
540 the northeast-trending flow, most gullies become inactive and the contourite channel is strongly
541 affected by the MU flow. The vertical shifts along the glacial/interglacial cycle of the interface between
542 the Mediterranean Water and the overlying ENACW (Fig. 2; Hernández-Molina et al., 2014, 2016;
543 Sánchez Leal et al., 2017) and the high variability of the water masses dynamics (Bellanco and Sánchez-
544 Leal, 2016; Roque et al., 2019) may also have favoured the incision of gullies.

545 LQD marks a change in the paleoclimatic and paleoceanographic conditions that influenced the
546 evolution of the plastered drift. After the initial stage of plastered drift growth and upslope migration
547 (Q6-a and Q6-b), a stage of aggradation occurred with deposition of the two more recent sub-units Q6-
548 c and Q6-d (Fig. 10). The most recent sub-unit Q6-d is incised by markedly asymmetric gullies
549 displaying northwestward migration in the Central area, which denotes increased bottom current
550 influence on the gravitational sediment transport. The predominance of contouritic processes versus
551 gravitational processes during deposition of this last sub-unit is also responsible for the inactivation
552 and infilling of many buried upper slope gullies. The mounded body infilling the erosional scour at the
553 shelf edge (Fig. 9b) suggests bottom current acceleration by the interaction with the escarpment
554 associated to the escarpment (e.g., Rebesco et al., 2014; Juan et al., 2020). The deposition of a
555 sediment wave field in the Northern area, which constitutes the main morphological difference with
556 the Central area (smooth inter-gullies areas; Fig. 5), is interpreted as a combination of sediment
557 deformation related to unconfined turbidite flows (Ercilla et al., 2002; García et al., 2012) and the
558 intensified effect of bottom currents (Faugères et al., 2000a,b; Gonthier et al., 2002), as indicated by
559 the orientation (parallel to oblique to bathymetric contours and to the bottom current direction) and
560 the upslope migration of sediment waves (Masson et al., 2002; Wynn and Stow, 2002). Bottom
561 currents intensification after the LQD may have been favored by the prevalence of glacial cycles with
562 longer and warmer interglacials (Roque et al., 2012), and is consistent with the transition from sandy
563 sheeted drifts to muddy sheeted and mounded drifts observed in the middle slope (Hernández-Molina
564 et al., 2016). Sediment waves development may also have been favored by high-energy processes

565 (eddies, internal tides or internal waves) associated to water masses interfaces (Cacchione et al., 2002;
566 Youbin et al., 2008; Lamb, 2014) as their location also coincides with the interface between the
567 ENACW and the MU (Fig. 3; Hernández-Molina et al., 2014, 2016; Sánchez-Leal et al., 2017; Roque et
568 al., 2019).

569 *5.3. Episodic pattern of tectonic deformation: Influence of tectonic deformation on sedimentary* 570 *processes*

571 The MPD marked a phase of tectonic activity in the region that resulted in the formation of
572 erosional surfaces close to diapirs and basement highs (Lofi et al., 2016; Hernández-Molina et al.,
573 2016). Tectonic activity evolved episodically since the MPD as shown by changes in the deformation of
574 seismic units and sub-units and the different development of morphological features in the seismic
575 record. During deposition of Q5 (MPD-LQD) sedimentation was controlled by the activity of marly and
576 salt diapirs rooted in the AUGC, under a compressive regime between Iberia and Africa (Maestro et al.,
577 2003; Medialdea et al., 2004), as indicated by the correlation between diapir distribution (Fig. 6) and
578 the thickness of seismic unit Q5 which infills depressed areas delimited by diapiric highs (Fig. 12a). The
579 upward deformation and thinning of sub-units indicate that diapir activity was coeval to Q5 deposition.

580 A prominent change of depositional conditions during deposition of sub-units Q6-a and Q6-b (LQD-
581 discontinuity 6c) is inferred by the absence of significant thickness variations in relation to NE-SW-
582 aligned buried diapirs in the upper slope, that would have become inactive (Figs. 7 to 11). The
583 decrease in diapiric activity in the upper slope may be coeval with the inactivation of some diapiric
584 ridges in the middle slope (Hernández-Molina et al., 2016). In contrast, the outcropping Cadiz diapiric
585 ridge (CDR) and the buried NW-SE-aligned diapirs continued or started to deform the sedimentary
586 units. In this scenario, mass flow deposits were formed at the foot of diapir-related faults (Figs. 9 and
587 10).

588 Tectonic activity can be related to the WNW-ESE strike-slip faults recognized in the Gulf of Cadiz,
589 with a dextral movement (Terrinha et al., 2009; García et al., 2009; Bartolomé et al., 2012; Martínez-
590 Loriente et al., 2014). During this stage (Q6-c) sedimentation changed drastically as it lacks most of the
591 structural imprint in the form of faults related to diapirs, except for the southernmost part of the study
592 area. In this scenario, mass flow deposits were formed at the foot of the faults. Although the
593 continuous uplift of NW-SE-oriented diapirs is suggested by the thinning of the sub-unit Q6-c on top of
594 the diapiric highs, it is less significant than in the other stages (Figs. 7 to 11). After the scarce diapiric
595 activity in the previous phase, deformation in sub-unit Q6-d is related to the activity of the
596 outcropping diapiric ridges and the buried NW-SE-oriented diapirs. This activity may explain the

597 instability event that created escarpments and the erosion of the previous sub-unit in the Southern
598 area (Fig. 10). The last sub-unit of Q6 (Q6-d; discontinuity 6d-surface) is only deformed by the CDR and
599 one of the NW-SE-oriented diapir alignments located in the area that limits the Central and Northern
600 areas. The outcropping Cadiz and Guadalquivir diapiric ridges are the only NE-SW structures that show
601 significant activity after the MPD. This can be explained by changes in the activity of faults, leading to a
602 northwestward displacement of tectonic activity after the MPD, but can be also favoured by
603 downbuilding (passive diapirism), that allows the continued growth of a diapir after it pierces the
604 surface, while sedimentat accumulates at its flanks (Barton, 1933; Jackson and Hudec, 2017). The
605 relative high/low sedimentation rate around/on the diapiric ridges, caused by the activity of bottom
606 currents, would originate the differential sedimentary burden, contributing to diapir growth.

607 Episodic tectonic deformation has influenced the sedimentary processes since the MPD, including:
608 1) bottom current deposition/erosion; 2) gravitational processes; and 3) fluid escape processes.

609 5.3.1. Tectonic influence on bottom current processes

610 Between the MPD and the LQD (seismic unit Q5) the plastered drift was deposited on the upper
611 slope, consisting of quite tabular and aggrading sub-units. Tectonic activity controlled the
612 accommodation space, as indicated by the distribution of depocenters in the depressions between
613 diapiric bodies (Fig. 12a). The paleo-channel was located about 6 km to the east from the present-day
614 Northern channel, whereas a wide terrace formed by gently upslope-prograding reflections was
615 deposited on the middle slope (Fig. 10a).

616 After the LQD, a number of processes including paleo-channel migration towards its present-day
617 position, the narrowing and/or westward displacement of the middle slope terrace and the basinward
618 migration of the plastered drift (Figs 7 to 12) could be related to tectonic activity of diapir-related
619 faults coeval with LQD. Diapiric activity uplifted the area bounding the Central and Northern areas. The
620 terrace-paleo-channel system migrated to a more distal position as it adjusted to the new margin
621 morphology, in a cooler climatic regime with probably deeper MOW/ENACW circulation. After the LQD
622 the plastered drift growth increased and depocenters migrated downslope, initially in the Central area
623 (sub-unit Q6-a; Fig. 10) and later in the Northern area (sub-unit Q6-b; Fig. 11). The plastered drift
624 growth is responsible for the unusual convex-upwards profile of the upper slope in the Central area
625 (Fig. 4b), that differs from the concave-upwards profile with marked gradient change between the
626 upper and middle slope in the rest of the margin. These lateral differences on the overall plastered
627 drift morphology could be explained by the relative higher dominance of gravitational processes over
628 bottom current processes along the upper slope. After the main pulse of basinward migration,

629 depocenters show a progressive displacement towards shallower positions (Figs. 10 and 11), in
630 agreement with the typical evolution of plastered drifts (Rebesco et al., 2014).

631 5.3.2. Tectonic influence on gravitational processes

632 Diapiric activity may be invoked as a trigger for mass-wasting processes, as uplift and faulting
633 associated with diapir intrusion may produce fracture and oversteepening of the slope that leads to
634 instability and failure (Cashman and Popenoe, 1985; Hampton et al., 1996). In the Cadiz upper slope,
635 arcuate- and linear-shaped escarpments along the shelf-edge can be related to the activity of a buried
636 diapir high and associated normal faults identified below in the sub-surface (Fig. 6). Moreover, the
637 increase in upper slope gradient induced by diapirs uplift can further favor gully incision (Mountjoy et
638 al., 2009; Argnani et al., 2011; Alves et al., 2014) as it is observed in the Central area. Furthermore,
639 diapir-rooted faults may produce topographic steps or lips along which gravitational flows are
640 channelized (Vargas et al., 2012; Micallef et al., 2014; Pellegrini et al., 2016; Tsai et al., 2018). This is
641 proposed to be the case of the gullies in the older seismic unit Q5, particularly in the Central area,
642 based on their spatial correlation with faults (Figs. 7 and 8). Subsequently, several Late Pleistocene and
643 Holocene reactivations of upper slope diapirism (Vázquez et al., 2010; Fernández-Puga et al., 2014)
644 could have favored continued gully development (Figs. 7 to 11), particularly in sub-unit Q6-c where
645 gullies are less developed and only occur associated to diapiric high-sic movements in the southern part
646 of the study area (Fig. 8a). Uplift of the Cadiz diapiric ridge forced the confinement of mass transport
647 deposits that occur as transparent to chaotic deposits in the most recent sub-unit Q6-d on the
648 shallower upper slope and at the limit between upper and middle slope in the Northern area (Fig. 11),
649 and may also have limited the gullies development in this area due to the decrease of the slope
650 gradient.

651 5.3.3. Tectonic influence on fluid escape processes

652 Fluid-escape features include circular- to elliptical-shaped depressions on the seafloor and depressions
653 in the seismic records (Figs. 7b and 8b). Depressions are distinguished from gullies based on the
654 circular- to elliptical plan-view shape for the seafloor features (Hovland and Judd, 1988; Schattner et
655 al., 2018), and the occurrence of acoustic amplitude anomalies in columnar shape and bright spots in
656 the seismic record (Plaza-Faverola et al., 2011; Cartwright and Santamarina, 2015; Maestrelli et al.,
657 2017). Indeed, evidences for fluid-escape related to active diapirism have been found in the Gulf of
658 Cadiz, resulting in the formation of pockmarks and blind valleys (Medialdea et al., 2009; León et al.,
659 2010). Fluid-escape may be controlled by diapiric faults, that form preferential conduits (Casas et al.,
660 2003; Somoza et al., 2003; Medialdea et al., 2004; Fernández-Puga et al., 2007; Medialdea et al., 2009;

661 Schattner et al., 2018). Fluid-escape features in the deeper upper slope of the Southern area (Figs. 5b,
662 7a and 8b) are located on top of buried diapir alignments that became inactive during the LQD,
663 although recent fluid-escape activity has been demonstrated by the identification of seeping bubbles
664 above some of the depressions (Baraza and Ercilla, 1996).

665

666 **6. Summary and conclusions**

667 The Cadiz upper and proximal middle slope have evolved since the Middle Pleistocene under the
668 major control of the tectonic activity, responsible for diapiric movements and associated faults, and
669 sea-level changes, that have determined the interplay between downslope (gravitational) and along-
670 slope (bottom current related) sedimentary processes. Two evolutionary stages are proposed (Fig. 13):

671 *a) Small, plastered drift deposition under the activity of NE-SW-oriented diapiric ridges (MPD-LQD; Fig.*
672 *13a).* A plastered drift developed in the Central area during the regressive and low sea-level stages of
673 glacial cycles, as the MU deepened and the upper slope was swept by the southeastward flow of the
674 ENACW. In the northern area, small patchy plastered drifts were deposited. The activity of NE-SW-
675 oriented diapiric bodies produced their deformation and the occurrence of mass flow processes such
676 as slope instability and gullies incision. A contourite terrace associated to the main MOW flow was
677 formed at the western side of the paleo-contourite channel.

678 *b) Plastered drift growth and upslope migration of sedimentation under the activity of NW-SE-oriented*
679 *buried diapirs (LQD-present; Fig. 13b).* At the LQD, most of the NE-SW-aligned buried diapirs in the
680 Central and Northern areas became inactive, but the activity of the outcropping diapiric ridges and the
681 buried NW-SE-aligned diapirs resulted in deformation of the deposits by faults and the occurrence of
682 mass-transport deposits related to slope instability. The results of this work suggest that adjustment to
683 the tectonic uplift of the area bounding the Central and Northern areas produced the migration of the
684 upper slope plastered drift and the terrace-channel system in the middle slope towards its present-day
685 position. The plastered drift developed significantly during this stage, probably as result of deep
686 currents enhancement and increased sediment supply during regressive and low sea-level stages.
687 Seismic unit Q6 records the upslope migration of the plastered drift. Tectonic activity was not
688 continuous, but a period of “quietness” led to low deformation and gully incision during deposition of
689 sub-unit Q6-c. This quiet period was followed by renewed tectonic activity of the outcropping diapiric
690 ridges and the NW-SE-oriented buried diapiric bodies, which produced instability events.

691 This work reveals a progressive change in diapiric activity, both in the orientation of active diapir
692 alignments along time and in the overall northwestward migration of deformation that is related with
693 the dynamics of the Allocthonous Unit of the Gulf of Cadiz. Diapiric deformation produced changes in

694 the accommodation space that was infilled by the predominant contouritic sedimentation, but also
695 changes in the upper slope physiography, that led to the occurrence of a variety of downslope mass
696 transport processes. The most important implications are: I) gullies incision favoured by the increase in
697 the slope and controlled by diapir-related faults, affected along their development by the
698 southeastward bottom currents; II) mass transport processes related to the activity of diapir-related
699 faults and probably further facilitated by the erosive effect of the bottom current; III) fluid-escape
700 features associated to faults rooted in the diapirs; IV) changes in the bottom current distribution,
701 forced to adjust to tectonically-induced changes in the margin morphology.

702 The results of this work highlight the two-ways-interaction between diapiric activity and
703 erosive/depositional bottom current related processes. Sedimentation in the Cadiz upper slope since
704 the Middle Pleistocene is strongly controlled by the activity of buried diapirs that accommodate the
705 ongoing deformation of the Allochthonous Unit. The continuous deformation of the outcropping diapirs
706 after the LQD, when most of the buried NE-SW-oriented structures were inactivated, may result from
707 their passive behavior favored by the lack of sedimentary cover, that in turns is the result of bottom
708 currents activity sweeping the study area, producing the erosion/non deposition over diapiric ridges
709 and the development of thick contouritic drifts in the areas between diapirs. Together with sea-level
710 changes, recent tectonic deformation is demonstrated as a key control in the development of
711 contouritic-gravitational systems, and has to be incorporated in the investigation of their reservoir
712 potential.

713 **Acknowledgements**

714 This work has been possible thanks to funding provided by the following projects funded by the
715 Spanish Ministry of Economy and Competitiveness: TALUS (CGL2015-74216-JIN), INPULSE (CTM2016-
716 75129-C3-1-R), CONTOURIBER (CTM2008-06399-04-04), MOWER (CTM-2012-395599-C03), SCORE
717 (CGL2016-80445-R; AEI/FEDER, UE), and FAUCES (CTM2015-65461-C2-1-R). We are very grateful to
718 REPSOL for allowing us to use an unpublished seismic line S81A-16 from the Gulf of Cadiz. The
719 investigation has been conducted within the framework of "The Drifters" Research Group (Royal
720 Holloway University of London). We are very grateful to Dr. Vittorio Maselli and Dr. Davide Gamboa for
721 their careful review of the manuscript and the helpful comments and suggestions. We also thank the
722 Associate Editor, Dr. Andrew Green, for his support in the publication process.

723 **References**

724

- 725 Akinci, L., Sawyer, D., 2016. Deriving the rate of salt rise at the Cape Fear slide using new seismic data.
726 In: Lamarche G. et al. (Eds.) Submarine Mass Movements and their Consequences. Advances in
727 Natural and Technological Hazards Research, Vol 41. Springer.

- 728 Alonso, B., Ercilla, G., Casas, D., Stow, D.A.V., Rodríguez-Tovar, F.J., Dorador, J., Hernández-Molina, F.J.,
729 2016. Contourite vs gravity-flow deposits of the Pleistocene Faro Drift (Gulf of Cadiz):
730 Sedimentological and mineralogical approaches. *Marine Geology* 377, 77–94.
- 731 Argnani, A., Tinti, S., Zaniboni, F., Pagnoni, G., Armigliato, A., Panetta, D., Tonini, R., 2011. The eastern
732 slope of the southern Adriatic basin: a case study of submarine landslide characterization and
733 tsunamigenic potential assessment. *Marine Geophysical Research* 32, 299–311.
- 734 Alves, T.M., Strasser, M., Moore, G.F., 2014. Erosional features as indicators of thrust fault activity
735 (Nankai Trough, Japan). *Marine Geology* 356, 5–18.
- 736 Baraza, J., Ercilla, G., Nelson, C.H., 1999. Potential geological hazards on the Eastern Gulf of Cadiz slope
737 (SW Spain). *Marine Geology* 155, 191–215.
- 738 Baraza, J., Ercilla, G., 1996. Gas-charged sediments and large pockmark-like features on the Gulf of
739 Cadiz (SW Spain). *Marine and Petroleum Geology* 13, 253–261.
- 740 Baringer, M.O., Price, J.F., 1999. A review of the physical oceanography of the Mediterranean Outflow.
741 *Marine Geology* 155, 63–82.
- 742 Bartolome, R., Gràcia, E., Stich, D., Martínez-Loriente, S., Klaeschen, D., Mancilla, F., Lo Iacono, C.,
743 Dañobeitia, J.J., Zitellini, N., 2012. Evidence for active strike-slip faulting along the Eurasia-Africa
744 convergence zone: Implications for seismic hazard in the southwest Iberian margin. *Geology* 40,
745 495–498.
- 746 Barton, D.C., 1933. Mechanics of formation of salt domes with special reference to Gulf coast salt
747 domes of Texas and Louisiana *American Association of Petroleum Geologist Bulletin* 17, 1025–1083.
- 748 Bellanco, M.J., Sánchez-Leal, R.F., 2016. Spatial distribution and intra-annual variability of water masses
749 on the Eastern Gulf of Cadiz seabed. *Continental Shelf Research* 128, 26–35.
- 750 Berndt, C., Cattaneo, A., Szuman, M., Trincardi, F., Masson, D., 2006. Sedimentary structures offshore
751 Ortona, Adriatic Sea – Deformation or sediment waves? *Marine Geology* 234, 261–270.
- 752 Borenäs, K.M., Wåhlin, A.K., Ambar, I., Serra, N., 2002. The Mediterranean outflow splitting- a
753 comparison between theoretical models and CANIGO data. *Deep-Sea Research II* 49, 4195–4205.
- 754 Brackenridge, R.E., Hernández-Molina, F.J., Stow, D.A.V., Llave, E., 2013. A Pliocene mixed contourite–
755 turbidite system offshore the Algarve Margin, Gulf of Cadiz: Seismic response, margin evolution and
756 reservoir implications. *Marine and Petroleum Geology* 46, 36–50.
- 757 Brackenridge, R.E., Stow, D.A.V., Hernández-Molina, F.J., Jones, C., Mena, A., Alejo, I., Ducassou, E.,
758 Llave, E., Ercilla, G., Nombela, M.A., Pérez-Arlucea, M., Frances, G., 2018. Textural characteristics
759 and facies of sand-rich contourite depositional systems. *Sedimentology* 65, 2223–2252.
- 760 Cacchione, D.A., Pratson, L.F., Ogston, A.S., 2002. The shaping of continental slopes by internal tides.
761 *Science* 296(5568), 724–727.
- 762 Campbell, D.C., Mosher, D.C., 2016. Geophysical evidence for widespread Cenozoic bottom current
763 activity from the continental margin of Nova Scotia, Canada. *Marine Geology* 378, 237–260.
- 764 Carter, L., Carter, R.M., 1988. Late Quaternary development of left-bank-dominant levees in the
765 Bounty Trough, New Zealand. *Marine Geology* 78, 185–197.
- 766 Cartwright, J., Santamarina, C., 2015. Seismic characteristics of fluid escape pipes in sedimentary
767 basins: Implications for pipe genesis. *Marine and Petroleum Geology* 65, 126–140.
- 768 Casas, D., Ercilla, G., Baraza, J., 2003. Acoustic evidences of gas in the continental slope sediments of
769 the Gulf of Cadiz (E Atlantic). *Geo-Marine Letters* 23, 300–310.
- 770 Cashman, K.V., Popenoe, P., 1985. Slumping and shallow faulting related to the presence of salt on the
771 continental slope and rise off North Carolina. *Marine and Petroleum Geology* 2, 260–271.
- 772 [Doi.org/10.1016/0264-8172\(85\)90016-9](https://doi.org/10.1016/0264-8172(85)90016-9).

- 773 de Castro, S., Hernández-Molina, F.J., Rodríguez-Tovar, F.J., Llave, E., Ng, Z.L., Nishida, N., Mena, A.,
774 2020. Contourites and bottom current reworked sands: Bed facies model and implications. *Marine*
775 *Geology* 428, doi.org/10.1016/j.margeo.2020.106267.
- 776 Diez, S., Gràcia, E., Gutscher, M.A., Matias, L., Mulder, T., Terrinha, P., Somoza, L., 2005. Bathymetric
777 map of the Gulf of Cadiz, NE Atlantic Ocean: The SWIM multibeam compilation. *Instrumentation*
778 *Viewpoint* 4, 42–43.
- 779 Ehlers, J., Gibbard, P.L., 2007. The extent and chronology of Cenozoic Global Glaciation. *Quaternary*
780 *International* 164, 6–20.
- 781 Ercilla, G., Alonso, B., Wynn, R.B., Baraza, J., 2002. Turbidity current sediment waves on irregular
782 slopes: observations from the Orinoco sediment-wave field. *Marine Geology* 192, 171–187.
- 783 Ercilla, G., Juan, C., Hernandez-Molina, F. J., Bruno, M., Estrada, F., Alonso, B., Casas, D., Farran, M.,
784 Llave, E., García, M., Vázquez, J.T. d'Acremont, E., Gorini, C., Palomino, D., Valencia, J., El Moumni,
785 B., Ammar, A., 2016. Significance of bottom currents in deep-sea morphodynamics: an example
786 from the Alboran Sea. *Marine Geology* 378, 157–170.
- 787 Ercilla, G., Juan, C., Periañez, R., Alonso, B., Abril, J. M., Estrada, F., Casas, C., Vázquez, J.T., d'Acremont,
788 E., Gorini, C., El Moumni, B., Do Couto, D., Valencia, J., 2019. Influence of alongslope processes on
789 modern turbidite systems and canyons in the Alboran Sea (southwestern Mediterranean). *Deep Sea*
790 *Research Part I: Oceanographic Research Papers* 144, 1–16.
- 791 Faugères, J.C., Gonthier, E., Stow, D.A.V., 1984. Contourite drift molded by deep Mediterranean
792 outflow. *Geology* 12, 296–300.
- 793 Faugères, J.C., Mézerais, M.L., Stow, D.A.V., 1993a. Contourite drift types and their distribution in the
794 North and South Atlantic Ocean basins. *Sedimentary Geology* 82, 189–203.
- 795 Faugères, J.C., Stow, D.A.V., 1993b. Bottom-current-controlled sedimentation: a synthesis of the
796 contourite problem. *Sedimentary Geology* 82, 287–297.
- 797 Faugères, J.C., Stow, D.A.V., Imbert, P., Viana, A., 1999. Seismic features diagnostic of contourite drifts.
798 *Marine Geology* 162, 1–38.
- 799 Faugères, J.C., Gonthier, E., Cirac, P., Castaing, P., Bellec, V., 2000a. Origine des dunes géantes
800 rencontrées sur le plateau Landais (Golfe de Gascogne). VIIème Colloque International
801 d'Océanographie du Golfe de Gascogne, Actes de Colloques, IFREMER 31, 26–31.
- 802 Faugères, J.C., Viana, A., Gonthier, E., Migeon, S., Stow, D.A.V., 2000b. Seismic features diagnostic of
803 contourite drifts and sediment waves. In: *Deep-Water Sedimentation: the Challenges for the Next*
804 *Millennium*, 31st IGC Workshop, Rio 2000, Deep-Seas, Abstr., pp. 26–32.
- 805 Fedele, J.J., García, M.H., 2009. Laboratory experiments on the formation of subaqueous depositional
806 gullies by turbidity currents. *Marine Geology* 258, 48–59.
- 807 Fernández-Salas, L.M., Sánchez-Rubio, N., Vázquez, J.T., Díaz del Río, V., López-González, N., Sánchez-
808 Leal, R., Bruque, G., López-Rodríguez, F.J., Palomino, D., Fernández-Puga, M., 2015. Geostatistical
809 analysis of the submarine channels in the upper slope of the Gulf of Cadiz (SW Iberian Peninsula).
810 *Resúmenes sobre el VIII Simposio MIA15*, Málaga.
- 811 Fernández-Puga, M.C., Vázquez, J.T., Somoza, L., Díaz del Río, V., Medialdea, T., Mata, M.P., León, R.,
812 2007. Gas-related morphologies and diapirism in the Gulf of Cadiz. *Geo-Marine Letters* 27, 213–
813 221.
- 814 Fernández-Puga, M.C., Vázquez, J.T., Medialdea, T., Somoza, L., Díaz del Río, V., León, R., 2010.
815 Morphological and geophysical evidences of tectonic activity in the Gulf of Cadiz northern
816 continental slope sector. *Iberian Meeting on Active Faults and Palaeoseismology*, Sigüenza, Spain.
817 Abstract volume, 159–162.

- 818 Fernández-Puga, M.C., Vázquez, J.T., Sánchez-Guillamón, O., Pajarón, L., Fernández-Salas, L.M.,
819 Palomino, D., Díaz del Río, V., 2014. Evidences of contemporary tectonic activity along the Eastern
820 Gulf of Cadiz continental shelf and upper slope. *Iberfault*, 2ª Reunión Ibérica sobre fallas activas y
821 paleosismología, Abstract Volume 85–88.
- 822 Field, M.E., Gardner, J.V., Prior, D.B., 1999. Geometry and significance of stacked gullies on the
823 northern California slope. *Marine Geology* 154, 271–286.
- 824 Fonnesu, M., Palermo, D., Galbiati, M., Marchesini, M., Bonamini, E., Bendias, D., 2020. A new world-
825 class deep-water play-type, deposited by the syndepositional interaction of turbidity flows and
826 bottom currents: The giant Eocene Coral Field in northern Mozambique. *Marine and Petroleum*
827 *Geology* 111, 179–201.
- 828 García, M., Hernández-Molina, F.J., Llave, E., Stow, D.A.V., León, R., Fernández-Puga, M.C., Díaz del Río,
829 V., Somoza, L., 2009. Contourite erosive features caused by the Mediterranean Outflow Water in
830 the Gulf of Cadiz: Quaternary tectonic and oceanographic implications. *Marine Geology* 257, 24–40.
- 831 García, M., Dowdeswell, J.A., Ercilla, G., Jakobsson, M., 2012. Recent glacially influenced sedimentary
832 processes on the East Greenland continental slope and deep Greenland Basin. *Quaternary Science*
833 *Reviews* 49, 64–81.
- 834 García, M., Hernández-Molina, F.J., Alonso, B., Vázquez, J.-T., Ercilla, G., Llave, E., Casas, D., 2016.
835 Erosive sub-circular depressions on the Guadalquivir Bank (Gulf of Cadiz): Interaction between
836 bottom current, mass-wasting and tectonic processes. *Marine Geology* 378, 5–19.
- 837 Gardner, J.V., Kidd, R.B., 1983. Sedimentary processes on the Iberian continental margin viewed by
838 long-range side-scan sonar. *Gulf of Cadiz. Oceanologica Acta* 6, 245–254.
- 839 Gong, C., Wang, Y., Zhu, W., Li, W., Xu, Q., 2013. Upper Miocene to Quaternary unidirectionally
840 migrating deep-water channels in the Pearl River Mouth Basin, northern South China Sea. *The*
841 *American Association of Petroleum Geologists Bulletin* 97, 285–308.
- 842 Gong, C., Wang, Y., Rebesco, M., Salon, S., Steel, R.J., 2018. How do turbidity flows interact with
843 contour currents in unidirectionally migrating deep-water channels? *Geology* 46, 551–554.
- 844 Gonthier, E.G., Faugeres, J.-C., Stow, D.A.V., 1984. Contourite facies of the Faro drift, Gulf of Cadiz. In:
845 Stow, D.A.V., Piper, D.J.W. (Eds.), *Fine-Grained Sediments: Deep-Water Processes and Facies*,
846 *Geological Society of London, Special Publications* 15, pp. 775– 797.
- 847 Gonthier, E., Faugères, J.C., Gervais, A., Ercilla, G., Alonso, B., Baraza, J., 2002. Quaternary
848 sedimentation and origin of the Orinoco sediment-wave field on the Demerara continental rise (NE
849 margin of South America). *Marine Geology* 192, 189–214.
- 850 Grundlingh, M.L., 1981. On the observation of a solitary event in the Mediterranean outflow west of
851 Gibraltar. *"Meteor" Forsch. Ergebn.* 23, 3–46.
- 852 Gütscher, M.-A., Dominguez, S., Westbrook, G.K., Gente, P., Babonneau, N., Mulder, T., Gonthier, E.,
853 Bartolome, R., Luis, J., Rosas, F., Terrinha, P., The Delila and DelSis Scientific Teams, 2009. Tectonic
854 shortening and gravitational spreading in the Gulf of Cadiz accretionary wedge: Observations from
855 multi-beam bathymetry and seismic profiling. *Marine and Petroleum Geology* 26, 647–659.
- 856 Gütscher, M.-A., Dominguez, S., Westbrook, G.K., Le Roy, P., Rosas, F., Duarte, J.C., Terrinha, P.,
857 Miranda, J.M., Graindorge, D., Gailler, A., Sallares, V., Bartolomé, R., 2012. The Gibraltar
858 subduction: A decade of new geophysical data. *Tectonophysics* 574-575, 72–91.
- 859 Hanquiez, V., Mulder, T., Toucanne, S., Lecroart, P., Bonnel, C., Marchès, E., Gonthier, E., 2010. The
860 sandy channel-lobe depositional systems in the Gulf of Cadiz: Gravity processes forced by contour
861 current processes. *Sedimentary Geology* 229, 110–123.
- 862 Hampton, M.A., Lee, H.J., Locat, J., 1996. Submarine landslides. *Reviews of Geophysics* 34, 33-59.

- 863 Haq, B.U., Hardenbol, J., Vail, P.R., 1987. Chronology of fluctuating sea levels since the Triassic.
864 Science 235, 1156–1167.
- 865 Hayward, B.W., Grenfell, H.R., Sabaa, A.T., Sikes, E.L., 2005. Deep-sea benthic foraminiferal record of
866 the Middle Pleistocene Climate Transition in the South-west Pacific. In: M. J. Head and P. L. Gibbard
867 (Eds.) Early Middle Pleistocene transitions: the land-ocean evidence. Geological Society (London),
868 Special Publication 247, pp. 85–115
- 869 Head, M.J., Gibbard, P.L., 2005. Early–Middle Pleistocene Transitions: The Land–Ocean Evidence.
870 Geological Society, London, Special Publications 247..
- 871 Hernández-Molina, F.J., Llave, E., Somoza, L., Fernandez-Puga, M., Maestro, A., Leon, R., Medialdea, T.,
872 Barnolas, A., García, M., del Rio, V., Fernandez-Salas, L., Vazquez, J., Lobo, F., Dias, J., Rodero, J. and
873 Gardner, J., 2003. Looking for clues to paleoceanographic imprints: A diagnosis of the Gulf of Cadiz
874 contourite depositional systems. *Geology* 31, 19–22.
- 875 Hernández-Molina, F.J., Llave, E., Stow, D.A.V., García, M., Somoza, L., Vazquez, J., Lobo, F., Maestro,
876 A., del Rio, V., Leon, R., Medialdea, T. and Gardner, J., 2006. The contourite depositional system of
877 the Gulf of Cadiz: A sedimentary model related to the bottom current activity of the Mediterranean
878 outflow water and its interaction with the continental margin. *Deep-Sea Research Part II-Topical
879 Studies in Oceanography* 53, 1420–1463.
- 880 Hernández-Molina, F.J., Llave, E., Preu, B., Ercilla, G., Fontan, A., Bruno, M., Serra, N., Gomiz, J.,
881 Brackenridge, R., Sierro, F., Stow, D.A.V., García, M., Juan, C., Sandoval, N., Arnaiz, A., 2014.
882 Contourite processes associated with the Mediterranean Outflow Water after its exit from the
883 Gibraltar Strait; global and conceptual implications. *Geology* 42, 231–234.
- 884 Hernández-Molina, F.J., Sierro, F.J., Llave, E., Roque, C., Stow, D.A.V., Williams, T., Lofi, J., Van der
885 Schee, M., Arnaiz, A., Ledesma, S., Rosales, C., Rodriguez-Tovar, F.J., Pardo-Iguzquiza, E. and
886 Brackenridge, R.E., 2016. Evolution of the Gulf of Cadiz margin and southwest Portugal contourite
887 depositional system: Tectonic, sedimentary and paleoceanographic implications from IODP
888 expedition 339. *Marine Geology* 337, 7–39.
- 889 Hovland, M., Judd, A.G., 1988. Seabed Pockmarks and Seepages: Geological Ecological and
890 Environmental Implication. Springer, 336 pp.
- 891 Howe, J.A., 1996. Turbidite and contourite sediment waves in the northern Rockall Trough, North
892 Atlantic Ocean, *Sedimentology* 43, 219–234.
- 893 Jackson, M.P.A., Hudec, M.R., 2017. Salt tectonics. Principles and practice. Cambridge University Press,
894 <https://doi.org/10.1017/9781139003988>.
- 895 Juan, C., Ercilla, G., Estrada, F., Alonso, B., Casas, D., Vázquez, J. T., d’Acremont, E., Medialdea, T.,
896 Hernández-Molina, F.J., Gorini, C., El Moumni, B., Valencia, J., 2020. Multiple factors controlling the
897 deep marine sedimentation of the Alboran Sea (SW Mediterranean) after the Zanclean Atlantic
898 Mega-flood. *Marine Geology* 423, 106138.
- 899 Kuvaas, B., Kristoffersen, Y., Leitchenkov, G., Guseva, J., Gandjukhin, V., 2004. Seismic expression of
900 glaciomarine deposits in the eastern Riiser Larsen Sea, Antarctica. *Marine Geology* 207, 1–15.
- 901 Lamb, K.G., 2014. Internal wave breaking and dissipation mechanisms on the continental slope/shelf.
902 *Annual Review of Fluid Mechanics* 46:231–54.
- 903 León, R., Somoza, L., Medialdea, T., Hernández-Molina, F.J., Vázquez, J.T., Díaz-del-Río, V., González,
904 F.J., 2010. Pockmarks, collapses and blind valleys in the Gulf of Cadiz. *Geo-Marine Letter* 30, 231–
905 247.
- 906 Li, H., Wang, Y., Zhu, W., Xu, Q., He, Y., Tang, W., Zhuo, H., Wang, D., Wu, J., Li, D., 2013. Seismic
907 characteristics and processes of the Plio-Quaternary unidirectionally migrating channels and

- 908 contourites in the northern slope of the South China Sea. *Marine and Petroleum Geology* 43, 370–
909 380.
- 910 Lisiecki, L.E., Raymo, M.E., 2005. A Pliocene-Pleistocene stack of 57 globally distributed benthic $\delta^{18}O$
911 records. *Paleoceanography* 20, doi.org/10.1029/2004PA001071.
- 912 Locker, S.D., Laine, E.P., 1992. Paleogene-Neogene depositional history of the middle U.S. Atlantic
913 continental rise: mixed turbidite and contourite depositional systems. *Marine Geology* 103, 137–
914 164.
- 915 Llave, E., Hernández-Molina, F.J., Somoza, L., Díaz-del-Río, V., Stow, D.A.V., Maestro, A., Alveirinho
916 Dias, J.M., 2001. Seismic stacking pattern of the Faro-Albufeira contourite system (Gulf of Cadiz): A
917 Quaternary record of paleoceanographic and tectonic influences. *Marine Geophysical Researches*
918 22, 487–508.
- 919 Llave, E., Schonfeld, J., Hernández-Molina, F.J., Mulder, T., Somoza, L., Díaz del Río, V. and Sanchez-
920 Almazo, I., 2006. High-resolution stratigraphy of the Mediterranean outflow contourite system in
921 the Gulf of Cadiz during the late Pleistocene: The impact of Heinrich events. *Marine Geology* 227,
922 241–262.
- 923 Llave, E., Hernández-Molina, F.J., Somoza, L., Stow, D.A.V., Díaz del Río, V., 2007a. Quaternary
924 evolution of the contourite depositional system in the gulf of Cadiz. In: Viana, A., Rebesco, M.
925 (Eds.), *Economic and Paleoceanographic Importance of Contourites*. Geological Society of London
926 Special Publication 276, pp. 49–79.
- 927 Llave, E., Hernández-Molina, F.J., Stow, D.A.V., Fernández-Puga, M.C., García, M., Vázquez, J.T.,
928 Maestro, A., Somoza, L., Díaz del Río, V., 2007b. Reconstructions of the Mediterranean Outflow
929 Water during the quaternary based on the study of changes in buried mounded drift stacking
930 pattern in the Gulf of Cadiz. *Marine Geophysical Researches* 28, 379–394.
- 931 Llave, E., Matias, H., Hernández-Molina, F.J., Ercilla, G., Stow, D.A.V., Medialdea, T., 2011. Pliocene and
932 Quaternary seismic stacking pattern and distribution of contourites in the Algarve margin (Northern
933 Gulf of Cadiz, Spain). *Geo-Marine Letters* 31, 377–390.
- 934 Llave, E., Hernández-Molina, F.J., García, M., de Weger, W., Ng, Z.L., Duarte, D., de Castro, S., Sierro,
935 F.J., Navas, J., 2019. Distribution of the Southern Contourite Channel (SE Gulf of Cadiz) since the
936 opening of the Strait of Gibraltar. 58th BSRG, London. Abstracts Volume.
- 937 Locker, S.D., Laine, E.P., 1992. Paleogene-Neogene depositional history of the middle U.S. Atlantic
938 Continental Rise; Mixed turbidite and contourite depositional systems. *Marine Geology* 103, 137–
939 164.
- 940 Lofi, J., Voelker, A.H.L., Ducassou, E., Hernández-Molina, F.J., Sierro, F.J., Bahr, A., Galvani, A., Lourens,
941 L.J., Pardo-Igúzquiza, E., Rodríguez-Tovar, F.J., William, T., 2016. Quaternary record in the gulf of
942 Cadiz and Portuguese contourite depositional systems. *Marine Geology* 377, 40–57.
- 943 Lonergan, L., Jamin, N.H., Jackson, C.A.-L., Johnson, H.D., 2013. U-shaped slope gully systems and
944 sediment waves on the passive margin of Gabon (West Africa). *Marine Geology* 337, 80–97.
- 945 Louarn, E., Morin, P., 2011. Antarctic Intermediate Water influence on Mediterranean Sea Water
946 outflow. *Deep Sea Research Part I: Oceanographic Research Papers* 58, 932–942.
- 947 Lopes, F.C., Cunha, P.P., Le Gall, B., 2006. Cenozoic seismic stratigraphy and tectonic evolution of the
948 Algarve margin (offshore Portugal, southwestern Iberian Peninsula). *Marine Geology* 231, 1–36.
- 949 Lozano, P. et al., 2020. Multiprocess interaction shaping geofoms and controlling substrate types and
950 benthic community distribution in the Gulf of Cadiz. *Marine Geology* 423, 106139.

- 951 Mack, G.H., 1978. The survivability of labile light mineral grains in fluvial, aeolian and littoral marine
952 environments: The Permian Cutler and Cedar Mesa Formation, Moab, Utah. *Sedimentology* 25,
953 587–606.
- 954 Madelain, F., 1970. Influence de la topographie du fond sur l'écoulement méditerranéen entre le
955 Détroit de Gibraltar et le Cap Saint-Vincent. *Cahiers Océanographiques* 22, 43–61.
- 956 Maestro, A., Somoza, L., Medialdea, T., Talbot, C.J., Lowrie, A., Vázquez, J.T., Díaz-del-Río, V., 2003.
957 Large-scale slope failure involving Triassic and Middle Miocene salt and shale in the Gulf of Cadiz
958 (Atlantic Iberian Margin). *Terra Nova* 15, 380–391.
- 959 Maestrelli, D., Iacopini, D., Jihad, A.A., Bond, C.E., Bonini, M., 2017. Seismic and structural
960 characterization of fluid escape pipes using 3D and partial stack seismic from the Loyal Field
961 (Scotland, UK): A multiphase and repeated intrusive mechanism. *Marine and Petroleum Geology*
962 88, 489–510.
- 963 Maldonado, A., Somoza, L., Pallares, L., 1999. The Betic orogen and the Iberian-African boundary in the
964 Gulf of Cadiz: geological evolution (central North Atlantic). *Marine Geology* 155, 9–43.
- 965 Marchès, E., Mulder, T., Cremer, M., Bonnel, C., Hanquiez, V., Gonthier, E., Lecroart, P., 2007.
966 Contourite drift construction influenced by capture of Mediterranean Outflow Water deep-sea
967 current by the Portimao submarine canyon (Gulf of Cadiz, South Portugal). *Marine Geology* 242,
968 247–260.
- 969 Marchès, E., Mulder, T., Gonthier, E., Cremer, M., Hanquiez, V., Garlan, T., Lecroart, P., 2010. Perched
970 lobe formation in the Gulf of Cadiz: Interactions between gravity processes and contour currents
971 (Algarve Margin, Southern Portugal). *Sedimentary Geology* 229, 81–94.
- 972 Martínez-Lorient, S., Sallarès, V., Gràcia, E., Bartolome, R., Dañoibeitia, J., Zitellini, N., 2014. Seismic
973 and gravity constraints on the nature. *Journal of Geophysical Research: Solid Earth* 119, 127–149.
- 974 Martorelli, E., Bosman, A., Casalbore, D., Falcini, F., 2016. Interaction of down-slope and along-slope
975 processes off Capo Vaticano (Southern Tyrrhenian Sea, Italy), with particular reference to
976 contourite-related landslides. *Marine Geology* 378, 43–55.
- 977 Maselli, V., Kneller, B., 2018. Bottom currents, submarine mass failures and halokinesis at the toe of
978 the Sigsbee Escarpment (Gulf of Mexico): contrasting regimes during lowstand and highstand
979 conditions? *Marine Geology* 401, 36–65.
- 980 Masson, D.G., Howe, J.A., Stoker, M.S., 2002. Bottom-current sediment waves, sediment drifts and
981 contourites in the northern Rockall Trough. *Marine Geology* 192, 215–237.
- 982 McAdoo, B.G., Pratson, L.F., Orange, D.L., 2000. Submarine landslide geomorphology, US continental
983 slope. *Marine Geology* 169, 103–136.
- 984 Medialdea, T., Vegas, R., Somoza, L., Vázquez, J.T., Maldonado, A., Díaz-del-Río, V., Maestro, A.,
985 Córdoba, D., Fernández-Puga, M.C., 2004. Structure and evolution of the “Olistostrome” complex of
986 the Gibraltar Arc in the Gulf of Cadiz (eastern Central Atlantic): evidence from two long seismic
987 cross-sections. *Marine Geology* 209, 173–198.
- 988 Medialdea, T., Somoza, L., Pinheiro, L., Fernandez-Puga, M., Vazquez, J., Leon, R., Ivanov, M.,
989 Magalhaes, V., Diaz-del-Rio, V. and Vegas, R., 2009. Tectonics and mud volcano development in the
990 Gulf of Cadiz. *Marine Geology* 261, 48–63.
- 991 Mestdagh, T., Lobo, F.J., Llave, E., Hernández-Molina, F.J., Van Rooij, D., 2019. Review of the late
992 Quaternary stratigraphy of the northern Gulf of Cadiz continental margin: New insights into
993 controlling factors and global implications. *Earth-Science Reviews* 198,
994 doi:10.1016/j.earscirev.2019.102944.

- 995 Mestdagh, T., Lobo, F.J., Llave, E., Hernández-Molina, F.J., García Ledesma, A., Puga-Bernabéu, A.,
996 Fernández-Salas, L.M., Van Rooij, D., 2020. Late Quaternary multi-genetic processes and products
997 on the northern Gulf of Cadiz upper continental slope (SW Iberian Peninsula). *Marine Geology* 427,
998 doi.org/10.1016/j.margeo.2020.106214.
- 999 Micallef, A., Mountjoy, J.J., 2011. A topographic signature of a hydrodynamic origin for submarine
1000 gullies. *Geology* 39, 115–118.
- 1001 Micallef, A., Mountjoy, J.J., Barnes, P.M., Canals, M., Lastras, G., 2014. Geomorphic response of
1002 submarine canyons to tectonic activity: Insights from the Cook Strait canyon system, New Zealand.
1003 *Geosphere* 10, 905–929.
- 1004 Michels, K.H., Kuhn, G., Hillenbrand, C.-D., Diekmann, B., Fütterer, D.K., Grobe, H., Uenzelmann-Neben,
1005 G., 2002. The southern Weddell Sea: combined contourite-turbidite sedimentation at the
1006 southeastern margin of the Weddell Gyre, in: Stow, D.A.V., Pudsey, C.J., Howe, J.A., Faugères, J.-C.,
1007 Viana, A.R. (Eds.), *Deep-Water Contourite Systems: Modern Drifts and Ancient Series, Seismic and*
1008 *Sedimentary Characteristics*. Geological Society, London, *Memoirs*, 22, pp. 305–323.
- 1009 Miramontes, E., Penven, P., Fierens, R., Droz, L., Toucanne, S., Jorry, S.J., Jouet, G., Pastor, L., Silva
1010 Jacinto, R., Gaillot, A., Giraudeau, J., Raisson, F., 2019. The influence of bottom currents on the
1011 Zambezi Valley morphology (Mozambique Channel, SW Indian Ocean): In situ current observations
1012 and hydrodynamic modelling. *Marine Geology* 410, 42–55.
- 1013 Miramontes, E., Eggenhuisen, J.T., Silva Jacinto, R., Poneti, G., Pohl, F., Normandeau, A., Campbell,
1014 D.C., Hernández-Molina, F.J., 2020. Channel-levee evolution in combined contour current-turbidity
1015 current flows from flume-tank experiments. *Geology* 48, doi.org/10.1130/G47111.1.
- 1016 Mountjoy, J.J., Barnes, P.M., Pettinga, J.R., 2009. Morphostructure and evolution of submarine
1017 canyons across an active margin: Cook Strait sector of the Hikurangi Margin, New Zealand: *Marine*
1018 *Geology* 260, 45–68.
- 1019 Mulder, T., Cochonat, P., 1996. Classification of offshore mass movements. *Journal of Sedimentary*
1020 *Research* 66, 43–57.
- 1021 Mulder, T., Faugères, J.C., Gonthier, E., 2008. Mixed Turbidite–Contourite Systems, in: Rebesco, M.,
1022 Camerlenghi, A. (Eds.), *Contourites. Developments in Sedimentology*. Elsevier, Amsterdam, 60, pp.
1023 435–456.
- 1024 Mulder, T., Lecroart, P., Hanquiez, V., Marches, E., Gonthier, E., Guedes, J.-C., Thiébot, E., Jaaidi, B.,
1025 Kenyon, N., Voisset, M., Pérez, C., Sayago, M., Fuchey, Y., Bujan, S., 2006. The western part of the
1026 Gulf of Cadiz: contour currents and turbidity currents interactions. *Geo-Marine Letters* 26, 31–41.
- 1027 Mulder, T., Gonthier, E., Lecroart, P., Hanquiez, V., Marchès, E., Voisset, M., 2009. Sediment failures
1028 and flows in the Gulf of Cadiz (eastern Atlantic). *Marine and Petroleum Geology* 26, 660–672.
- 1029 Nelson, C.H., Baraza, J., Maldonado, A., 1993. Mediterranean Undercurrent Sandy Contourites, Gulf of
1030 Cadiz, Spain. *Sedimentary Geology* 82, 103–131.
- 1031 Nelson, C.H., Baraza, J., Maldonado, A., Rodero, J., Escutia, C., Barber Jr., J.H., 1999. Influence of the
1032 Atlantic inflow and Mediterranean outflow currents on Late Quaternary sedimentary facies of the
1033 Gulf of Cadiz continental margin. *Marine Geology* 155, 99–129.
- 1034 Nelson, C.H., Maldonado, A., 1988. Factors controlling depositional patterns of Ebro turbidite systems,
1035 Mediterranean Sea. *American Association of Petroleum Geologists Bulletin* 72, 698–716.
- 1036 Ochoa, J., Bray, N.A., 1991. Water mass exchange in the Gulf of Cadiz. *Deep-Sea Research* 38, S465–
1037 S503.
- 1038 Palomino, D., López-González, N., Vázquez, J.-T., Fernández-Salas, L.-M., Rueda, J.L., Sánchez-Leal, R.,
1039 Díaz-del-Río, V., 2016. Multidisciplinary study of mud volcanoes and diapirs and their relationship to

- 1040 seepages and bottom currents in the Gulf of Cadiz continental slope (northeastern sector). *Marine*
1041 *Geology* 378, 196–212.
- 1042 Pellegrini, C., Maselli, V., Trincardi, F., 2016. Pliocene–Quaternary contourite depositional system along
1043 the south-western Adriatic margin: changes in sedimentary stacking pattern and associated bottom
1044 currents. *Geo-Marine Letters* 36, 67–70.
- 1045 Piper, D.J.W., Mosher, D.C., Campbell, D.C., 2012. Controls on the distribution of major types of
1046 submarine landslides. In: Clague, J.J. and Stead, D. (Eds.), *Landslides: types, mechanisms, and*
1047 *modeling*. Cambridge University Press, pp. 95–107.
- 1048 Platt, J.P., Allerton, S., Kirker, A., Mandeville, C., Mayfield, A., Platzman, E.S., Rimi, A., 2003. The
1049 ultimate arc: differential displacement, oroclinal bending, and vertical axis rotation in the External
1050 Betic-Rif arc. *Tectonics* 22, 1017, doi:10.1029/2001TC001321.
- 1051 Platt, J.P., Behr, W.M., Johannesen, K., Williams, J.R., 2013. The Betic-Rif Arc and its orogenic hinterland:
1052 a review. *Annual Review of Earth and Planetary Sciences* 41, 313–357.
- 1053 Plaza-Faverola, A., Bünz, S., Mienert, J., 2011. Repeated fluid expulsion through sub-seabed chimneys
1054 offshore Norway in response to glacial cycles. *Earth and Planetary Science Letters* 305, 297–308).
- 1055 Posamentier, H.W., Martinsen, O.J., 2010. The character and genesis of submarine mass-transport
1056 deposits: insights from outcrop and 3D seismic data. *SEPM Special Publications* 95, 7–38.
- 1057 Rasmussen, S., Lykke-Andersen, H., Kuijpers, A., Troelstra, S.R., 2003. Post-Miocene sedimentation at
1058 the continental rise of Southeast Greenland: the interplay between turbidity and contour currents.
1059 *Marine Geology* 196, 37–52.
- 1060 Rebesco, M., Pudsey, C.J., Canals, M., Camerlenghi, A., Barker, P.F., Estrada, F., Giorgetti, A., 2002.
1061 Sediment drifts and deep-sea channel systems, Antarctic Peninsula Pacific Margin, in: Stow, D.A.V.,
1062 Pudsey, C.J., Howe, J.A., Faugères, J.-C., Viana, A.R. (Eds.), *Deep-Water Contourite Systems: Modern*
1063 *Drifts and Ancient Series, Seismic and Sedimentary Characteristics*. Geological Society, London,
1064 *Memoirs*, 22, pp. 353–371.
- 1065 Rebesco, M., Hernández-Molina, F.J., Van Rooij, D., Wåhlin, A., 2014. Contourites and associated
1066 sediments controlled by deep-water circulation processes: State-of-the-art and future
1067 considerations. *Marine Geology* 352, 111–154.
- 1068 Richards, M., Bowman, M. and Reading, H. 1998. Submarine-fans systems I: Characterization and
1069 stratigraphic prediction. *Marine and Petroleum Geology* 15, 689–717.
- 1070 Rinke-Hardekopft, L., Reuning, L., Bourget, J., Back, S., 2018. Syn-sedimentary deformation as a
1071 mechanism for the initiation of submarine gullies on a carbonate platform to slope transition,
1072 Browse Basin, Australian North West Shelf. *Marine and Petroleum* 91, 622–630.
- 1073 Rodero, J., Pallarés, L., Maldonado, A., 1999. Late Quaternary seismic facies of the Gulf of Cadiz
1074 Spanish margin: depositional processes influenced by sea-level change and tectonic controls.
1075 *Marine Geology* 155, 131–156.
- 1076 Rodríguez, K., Hodgson, N., 2019. Hydrocarbon potential of hybrid depositional systems. *GEOExPro* 16,
1077 44–46.
- 1078 Roque, C., Duarte, H., Terrinha, P., Valadares, V., Noiva, J., Cahão, M., Ferreira, J., Legoínha, P., Zitellini,
1079 N., 2012. Pliocene and Quaternary depositional model of the Algarve margin contourite drifts (Gulf
1080 of Cadiz, SW Iberia): seismic architecture, tectonic control and paleoceanographic insights. *Marine*
1081 *Geology* 303–306, 42–62.
- 1082 Roque, D., Parras-Berrocal, I., Bruno, M., Sánchez-Leal, R., Hernández-Molina, F.J., 2019. Seasonal
1083 variability of intermediate water masses in the Gulf of Cadiz: implications of the Antarctic and
1084 subarctic seesaw. *Ocean Science* 15, 1–17.

- 1085 Rosenbaum, G., Lister, G., Duboz, C., 2002. Reconstruction of the tectonic evolution of the western
1086 Mediterranean since the Oligocene. *Journal of the Virtual Explorer* 8, 107–130.
- 1087 Ruano, P., Bohoyo, F., Galindo-Zaldívar, J., Pérez, L.F., Hernández-Molina, F.J., Maldonado, A., García,
1088 M., Medialdea, T., 2014. Mass transport processes in the Southern Scotia Sea: evidence of
1089 paleoearthquakes. *Global and Planetary Change* 123, 374-391.
- 1090 Ryan, W. B. F., Carbotte, S.M., Coplan, J., O'Hara, S., Melkonian, A., Arko, R., Weissel, R.A., Ferrini, V.,
1091 Goodwillie, A., Nitsche, F., Bonczkowski, J., Zemsky, R., 2009. Global Multi-Resolution Topography
1092 (GMRT) synthesis data set. *Geochemistry, Geophysics. Geosystems* 10, Q03014,
1093 doi:10.1029/2008GC002332.
- 1094 Sánchez-Leal, R.F., Bellanco, M.J., Fernández-Salas, L.M., García-Lafuente, J., Gasser-Rubinat, M.,
1095 González-Pola, C., Hernández-Molina, F.J., Pelegrí, J.L., Peliz, A., Relvas, P., Roque, D., Ruiz-Villarreal,
1096 M., Sammartino, S., Sánchez-Garrido, J.C., 2017. The Mediterranean Overflow in the Gulf of Cadiz: A
1097 rugged journey. *Science Advances* 3:eaa0609.
- 1098 Sánchez-Rubio, N., Fernández-Salas, L.M., Vázquez, J.T., Díaz del Río, V., López-González, N., Sánchez-
1099 Leal, R., Bruque, G., López-Rodríguez, F.J., Palomino, D., Fernández-Puga, M.C., 2015.
1100 Morphological characterization of submarine channels in the upper slope of the Gulf of Cadiz (SW
1101 Iberian Peninsula). *Resúmenes sobre el VIII Simposio MIA15*, Málaga.
- 1102 Sansom, P., 2018. Hybrid turbidite–contourite systems of the Tanzanian margin. *Petroleum Geoscience*
1103 24, 258–276.
- 1104 Schattner, U., Lobo, F.J., García, M., Kanari, M., Ramos, R.B., de Mahiques, M.M., 2018. A detailed look
1105 at diapir piercement onto the ocean floor: New evidence from Santos Basin, offshore Brazil. *Marine*
1106 *Geology* 406, 98–108.
- 1107 Serra, C.S., Martínez-Lorient, S., Gràcia, E., Urgeles, R., Vizcaino, A., Perea, H., Bartolome, R., Pallàs,
1108 R., Lo Iacono, C., Diez, S., Dañobeitia, J., Terrinha, P., Zitellini, N., 2020. Tectonic evolution,
1109 geomorphology and influence of bottom currents along a large submarine canyon system: The São
1110 Vicente Canyon (SW Iberian margin). *Marine Geology* 426, doi: [10.1016/j.margeo.2020.106219](https://doi.org/10.1016/j.margeo.2020.106219).
- 1111 Serra, N., Ambar, I., Käse, R., 2005. Numerical modelling of the Mediterranean Water splitting and
1112 eddy generation, *Deep-Sea Research I* 52, 383–408.
- 1113 Serra, N., Ambar, I., Boutov, D., 2010. Surface expression of Mediterranean Water dipoles and their
1114 contribution to the shelf/slope – open ocean exchange. *Ocean Science* 6, 191–209.
- 1115 Shanmugam, G., 2007. The obsolescence of deep-water sequence stratigraphy in petroleum geology.
1116 *Indian Journal of Petroleum Geology* 16, 1–45.
- 1117 Shanmugam, G., 2012. *New Perspectives on Deep-Water Sandstones: Origin, Recognition, Initiation,*
1118 *and Reservoir Quality*. Elsevier, Oxford, 544 pp.
- 1119 Somoza, L., Diaz-del-Rio, V., Leon, R., Ivanov, M., Fernandez-Puga, M., Gardner, J., Hernández-Molina,
1120 F.J., Pinheiro, L., Rodero, J., Lobato, A., Maestro, A., Vazquez, J., Medialdea, T. and Fernandez-Salas,
1121 L., 2003. Seabed morphology and hydrocarbon seepage in the Gulf of Cadiz mud volcano area:
1122 Acoustic imagery, multibeam and ultra-high resolution seismic data. *Marine Geology* 195, 153–176.
- 1123 Somoza, L., Lowrie A., Maestro, A., 1999. Allochthonous Blocks as Hydrocarbon Traps in the Gulf of
1124 Cadiz. *Offshore Technology Conference* 31, Vol. 1, 571–577.
- 1125 Spinelli, G., Field, M.E., 2001. Evolution of continental slope gullies on the Northern California. *Journal*
1126 *of Sedimentary Research* 71, 237–245.
- 1127 Teixeira, M., Terrinha P., Roque C., Rosa M., Ercilla G., Casas D., 2019. Interaction of along-slope and
1128 downslope processes in the Alentejo Margin (SW Iberia) - Implications on slope stability. *Marine*
1129 *Geology* 410, 88–108.

- 1130 Terrinha, P., Ribeiro, C., Kullberg, J.C., Rocha, R., Ribeiro, A., 2002. Compression episodes during rifting
1131 and faunal isolation in the Algarve Basins, SW Iberia. *Journal of Geology* 110, 101–113.
- 1132 Terrinha, P., Matias, L., Vicente, J., Duarte, J., Pinhero, L., Lourenço, N., Diez, S., Rosas, F., Magalhaes,
1133 V., Valadares, V., Zitellini, N., Roque, C., Mendes Víctor, L., MATESPRO Team, 2009.
1134 Morphotectonics and strain partitioning at the Iberia-Africa plate boundary from multibeam and
1135 seismic reflection data. *Marine Geology* 267, 165–174.
- 1136 Thorpe, S.A., 1976. Variability of the Mediterranean undercurrent in the Gulf of Cadiz. *Deep-Sea*
1137 *Research* 23, 711–727.
- 1138 Torelli, L., Sartori, R., Zitellini, N., 1997. The giant chaotic body in the Atlantic ocean off Gi-braltar: new
1139 results from a deep seismic reflection survey. *Marine and Petroleum Geology* 14, 125–138.
- 1140 Toucanne, S., Mulder, T., Schönfeld, J., Hanquiez, V., Gonthier, E., Duprat, J., Cremer, M., Zaragosi, S.,
1141 2007. Contourites of the Gulf of Cadiz: A high-resolution record of the paleocirculation of the
1142 Mediterranean outflow water during the last 50,000 years. *Palaeogeography, Palaeoclimatology,*
1143 *Palaeoecology* 246, 354–336.
- 1144 Tripsanas, E.K., Bryant, W.R., Prior, D.B., Phaneuf, B.A., 2003. Interplay Between Salt Activities and
1145 Slope Instabilities, Bryant Canyon Area, Northwest Gulf of Mexico, in: Locat, J., Mienert, J., Boisvert,
1146 L. (Eds.), *Submarine Mass Movements and Their Consequences: 1st International Symposium.*
1147 Springer Netherlands, Dordrecht, pp. 307–315.
- 1148 Tripsanas, E.K., Bryant, W.R., Phaneuf, B.A., 2004. Slope-instability processes caused by salt
1149 movements in a complex deep-water environment, Bryant Canyon area, northwest Gulf of Mexico.
1150 *The American Association of Petroleum Geologists Bulletin* 88, 801–823.
- 1151 Tsai, C.-H., Huang, C.-L., Hsu, S.-K., Doo, W.-B., Lin, S.-S., Wang, S.-Y., Lin, J.-Y., Liang, C.-W., 2018.
1152 Active normal faults and submarine landslides in the Keelung Shelf off NE Taiwan. *Terrestrial,*
1153 *Atmospheric and Oceanic Sciences* 29, 31–38.
- 1154 Twichell, D.C., Chaytor, J.D., ten Brink, U.S., Buczkowski, B., 2009. Morphology of late Quaternary
1155 landslides along the U.S. Atlantic continental margin. *Marine Geology* 264, 4–15.
- 1156 Van Rooij, D., Iglesias, J., Hernández-Molina, F.J., Ercilla, G., Gomez-Ballesteros, M., Casas, d., Llave, E.,
1157 De Hauwere, A., Garcia-Gil, S., Acosta, J., Henriot, J.-P., 2010. The Le Danois Contourite Depositional
1158 System: Interactions between the Mediterranean Outflow Water and the upper Cantabrian slope
1159 (North Iberian margin). *Marine Geology* 274, 1–20.
- 1160 Vargas, C.A., Mann, P., Gómez, C., 2012. Morphologic expression of accretionary processes and recent
1161 submarine landslides along the Southwestern Pacific Margin of Colombia. In: Yamada, Y.,
1162 Kawamura, K., Ikehara, K., Ogawa, Y., Urgeles, R., Mosher, D., Chaytor, J., Strasser, M. (Eds.),
1163 *Submarine Mass Movements and Their Consequences.* Springer, Netherlands, pp. 365–377.
- 1164 Vázquez, J.-T., López-González, N., Fernández-Salas, L., Díaz del Río, V., Fernández-Puga, M.C.,
1165 Palomino, D., Mata, M.P., Bárcenas, P., Sayago-Gil, M., Bruque, G., 2010. Nuevos datos de
1166 actividad tectónica durante el Pleistoceno Superior-Holoceno en el sector oriental de la plataforma
1167 continental del Golfo de Cadiz (SO de Iberia). In: Insúa, J.M., Martín-González, F. (Eds.),
1168 *Contribución de la Geología al Análisis de la Peligrosidad Sísmica.* DOI: 10.13140/2.1.3265.0245.
- 1169 Viana, A.R., 2009. Economic Relevance of Contourites. In: Rebesco, M., Camerlenghi, A. (Eds.),
1170 *Contourites. Developments in Sedimentology,* pp. 493–510.
- 1171 Wynn, R.B., Stow, D.A.V., 2002. Classification and characterisation of deep-water sediment waves.
1172 *Marine Geology* 192, 7–22.
- 1173 Youbin, H., Zhengzhong, G., Jinxiong, L., Shunshu, L., Xuefeng, L., 2008. Characteristics of internal-wave
1174 and internal-tide deposits and their hydrocarbon potential. *Petroleum Science* 5, 37–44.

1175 Zenk, W. ,1975. On the Mediterranean outflow west of Gibraltar. Meteor Forschungsergeb 16, 23–34.
1176

Journal Pre-proof

1177 Figure Captions

1178 Figure 1. a) Regional bathymetric map of the Gulf of Cadiz contourite depositional system showing the
 1179 main MOW cores and branches. ML: Mediterranean Lower core; MU: Mediterranean Upper
 1180 core; SB: Southern branch; PB: Principal branch; IB: Intermediate branch; 1: proximal scour and
 1181 sand ribbons sector; 2: active contourite drift sector; CC: Contourite channel; SD: Sheeted drift;
 1182 GDR: Guadalquivir diapiric ridge; CDR: Cadiz diapiric ridge; b) Datasets used in this work include
 1183 the swath bathymetric mosaic and airgun and multichannel seismic lines.

1184 Figure 2. a) Flow distribution of the MOW along the upper and middle slope. Flow direction and
 1185 velocity is taken from Sánchez-Leal et al. (2017); CC: Contourite channel; b) Hydrographic
 1186 profiles showing the distribution of the East North Antarctic Central Water (ENACW) and the
 1187 Mediterranean Outflow Water (MOW) that affect at present day the Cadiz upper and middle
 1188 slope (modified from Sánchez-Leal et al., 2017).

1189 Figure 3. a) Bathymetric map of the study area showing the location of the correlated profiles in b) and
 1190 c); CC: Contourite Channel (N: Northern; S: Southern; T: Tofiño; G: Gusano; H: Huelva; C: Cadiz);
 1191 CDR: Cadiz diapiric ridge; GDR: Guadalquivir diapiric ridge; b) airgun line CADIZ21; c)
 1192 multichannel line S81A-16, modified from Hernández-Molina et al. (2014, 2016), from which the
 1193 Mid-Pleistocene Discontinuity (MPD) and Late Quaternary Discontinuity (LQD) have been taken.
 1194 d) Table showing the links between the seismic units and sub-units from this work with previous
 1195 stratigraphic units and discontinuities. The units and sub-units are tentatively correlated with
 1196 the climatic record represented by the benthic $\delta^{18}O$ isotopic curve of Lisiecki and Raymo (2005).

1197 Figure 4. Physiographic characterization of the Gulf of Cadiz continental margin close to the Strait of
 1198 Gibraltar. a) Bathymetric map showing the physiographic domains, the location of the study
 1199 area and the three major areas (Southern, Central and Northern) considered in this work; b)
 1200 Bathymetric profiles from the outer continental shelf down to the proximal middle slope. See
 1201 location in a and b).

1202 Figure 5. a) Bathymetry of the continental margin showing the location of the study area and the
 1203 bathymetry and profiles shown in Fig.5b to Fig.5e; b) 3D model of the study area showing the
 1204 Southern, Central and Northern areas considered in this work; c) Detail of the bathymetric map
 1205 showing sediment waves; c) Detail of the bathymetric map showing the sediment waves in the
 1206 Northern area; d) shelf-edge escarpment and its bathymetric profile; e) Topographic profiles
 1207 across the slope gullies.

1208 Figure 6. a) Map of the basement depth, showing the main features that include two NE-SW-oriented
 1209 depressions and small basins. Outcropping diapirs are shown in orange colors, and white dots
 1210 represent the top of buried diapirs. This figure shows the two main orientations of these aligned
 1211 diapirs, NW-SE and NE-SW; CC: Contourite Channel; CDR: Cadiz diapiric ridge; GDR: Guadalquivir
 1212 diapiric ridge; b) Multichannel seismic profiles showing the basement, diapirs and faults in a
 1213 downslope direction.

1214 Figure 7. Shallower airgun profiles in orientations parallel to the isobaths and their interpretation. The
 1215 seismic units and sub-units and their seismic character is detailed, as well as the features
 1216 identified in the profiles (faults, gullies, chaotic-transparent deposits). The alignment of diapir

1217 tops are shown. Orange: NE-SW-oriented diapirs. Blue: NW-SW-oriented diapirs. CDR: Cadiz
1218 diapiric ridge; GDR: Guadalquivir diapiric ridge.

1219 Figure 8. Deeper airgun profiles in orientations parallel to the isobaths and their interpretation. The
1220 seismic units and sub-units and their seismic character is detailed, as well as the features
1221 identified in the profiles (faults, gullies, chaotic-transparent deposits). The alignment of diapir
1222 tops are shown. Orange: NE-SW-oriented diapirs. Blue: NW-SW-oriented diapirs. CDR: Cadiz
1223 diapiric ridge; GDR: Guadalquivir diapiric ridge.

1224 Figure 9. a) Bathymetric map showing the location of the airgun profiles shown in Fig. 9b, Fig. 10 and
1225 Fig. 11 and the position of buried and outcropping diapirs. Orange: NE-SW-oriented diapirs.
1226 Blue: NW-SW-oriented diapirs; b) Airgun profile and stratigraphic interpretation orientated
1227 perpendicular to the isobaths in the Southern area. The seismic units and sub-units and their
1228 seismic character is detailed, as well as the features identified in the profiles. See location and
1229 legends in a).

1230 Figure 10. Airgun profile and stratigraphic interpretation orientated perpendicular to the isobaths in
1231 the Central area. The seismic units and sub-units and their seismic character is detailed, as well
1232 as the features identified in the profiles. The mounded-prograding deposits in sub-unit Q6-c is
1233 detailed in the zoomed image. See location and legends in Fig. 9a.

1234 Figure 11. Airgun profile and stratigraphic interpretation orientated perpendicular to the isobaths in
1235 the Northern area. The seismic units and sub-units and their seismic character is detailed, as
1236 well as the features identified in the profiles. See location and legends in Fig. 9a; HCC: Huelva
1237 contourite channel.

1238 Figure 12. Isochore maps highlighting the distribution of depocenters of the two main seismic units
1239 and topography of their base (MPD: Mid Pleistocene Discontinuity; LQD; Late Quaternary
1240 Discontinuity) and isochore maps of the sub-units depocenters. CDR: Cadiz diapiric ridge; GDR:
1241 Guadalquivir diapiric ridge. The present-day location of the shelf break (discontinuous dark blue
1242 line) and main contourite channels (CC, in pink) along the middle slope is included as a
1243 reference.

1244 Figure 13. Sketches of the diapiric activity, bottom current distribution and sedimentary processes
1245 along the two stages of evolution of the Gulf of Cadiz continental margin in the area close to the
1246 Strait of Gibraltar: a) Mid Pleistocene Discontinuity to Late Quaternary Discontinuity; b) Late
1247 Quaternary Discontinuity to Present. The base topography of the base of unit Q5 (MPD) and Q6
1248 (LQD) are shown for reference.

1249

The role of late Quaternary tectonic activity and sea-level changes on sedimentary processes interaction in the Gulf of Cadiz upper and middle continental slope (SW Iberia)

García, M., Llave, E., Hernández-Molina, F.J., Lobo, F.J., Ercilla, G., Alonso, B., Casas, D., Mena, A., Fernández-Salas, L.M.

Highlights

- We show diapiric activity and sea-level control on sedimentation in the Gulf of Cadiz
- A plastered drift was deposited during lowstands on the ENACW-affected upper slope
- A contourite channel was incised in the proximal middle slope by the MOW
- Since the Late Quaternary diapiric activity changed its trend and migrated to the NW
- Sedimentary processes adapted to the margin morphology created by diapir activity

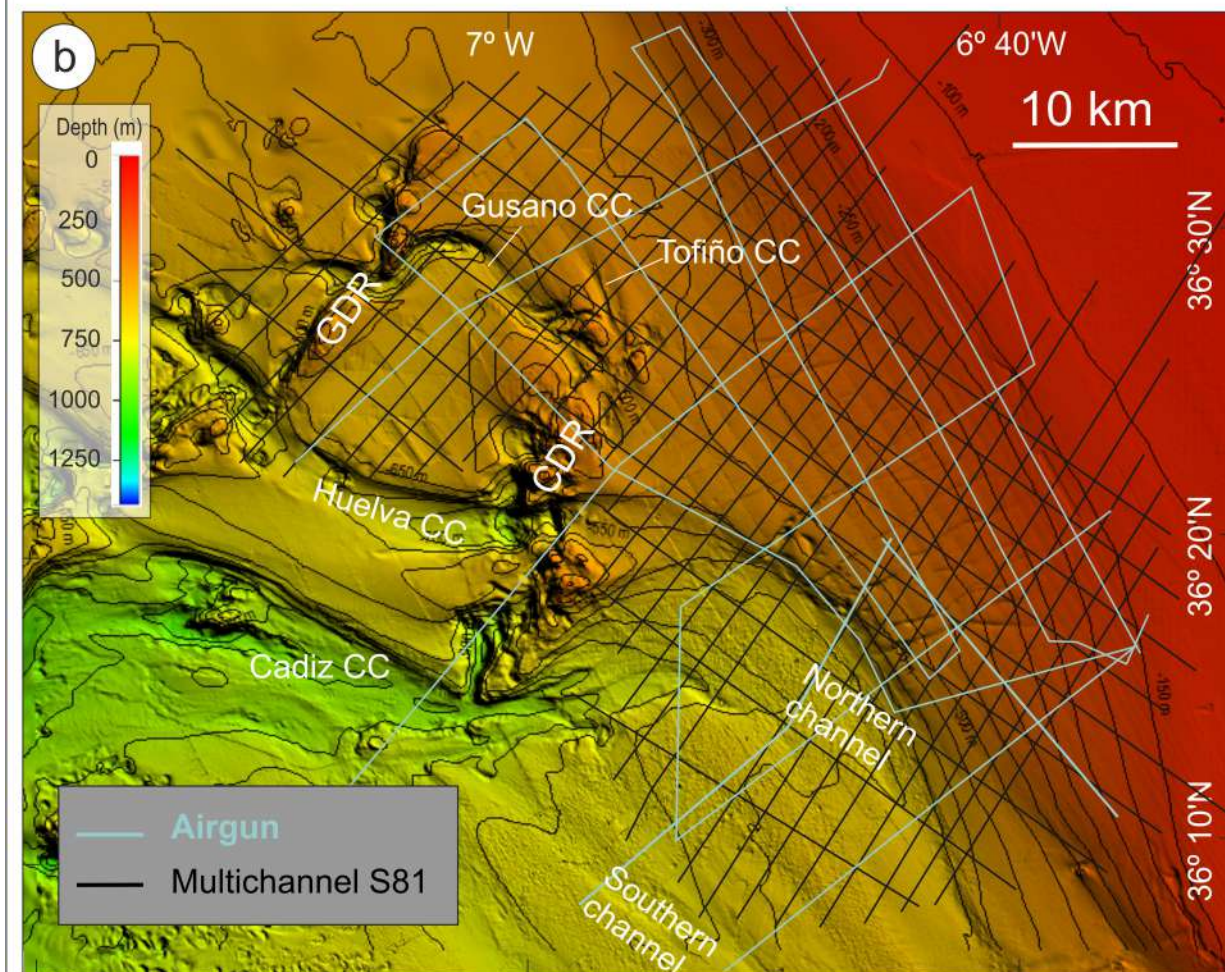
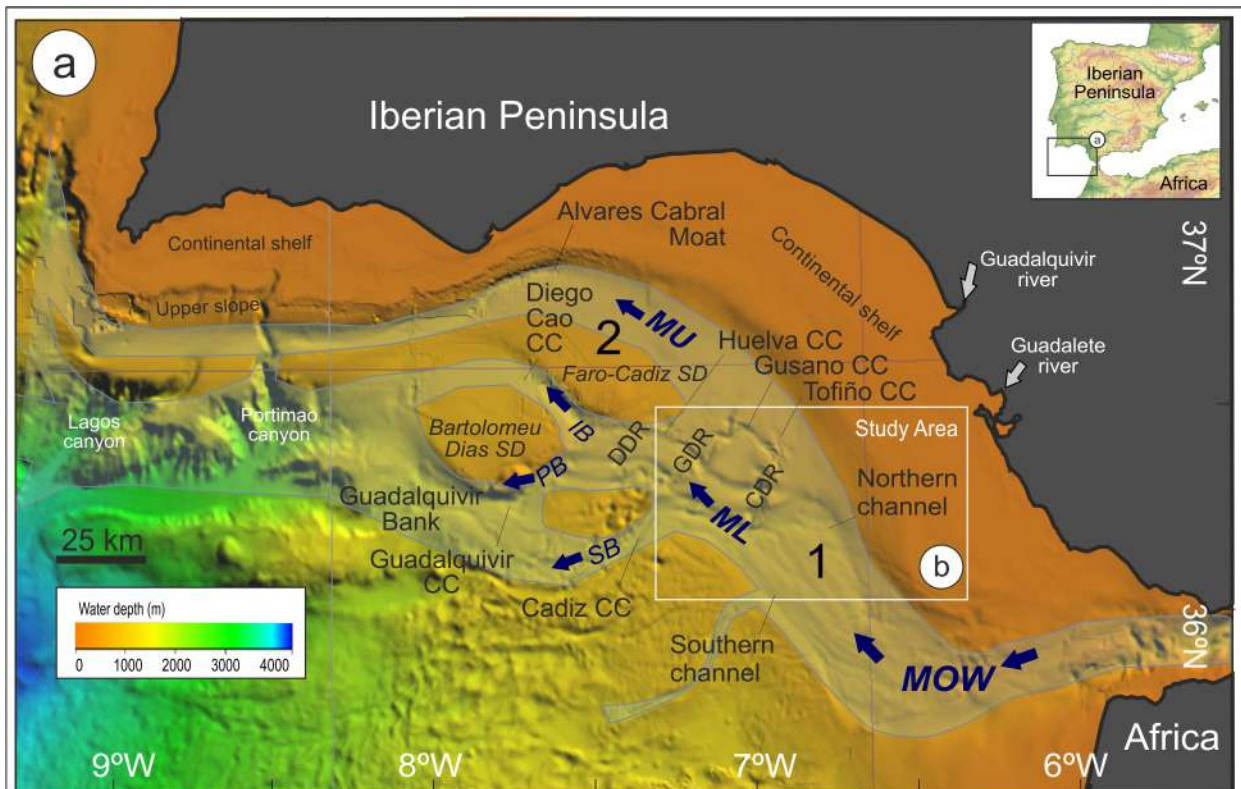
Declaration of interests

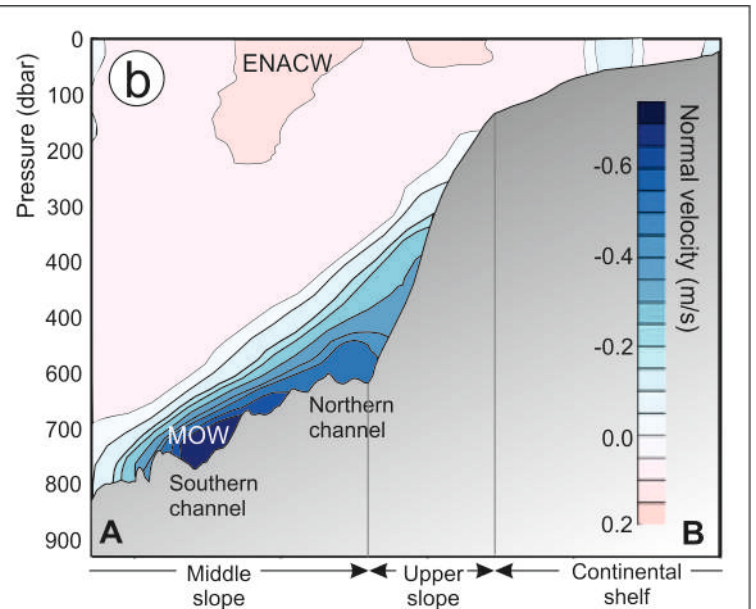
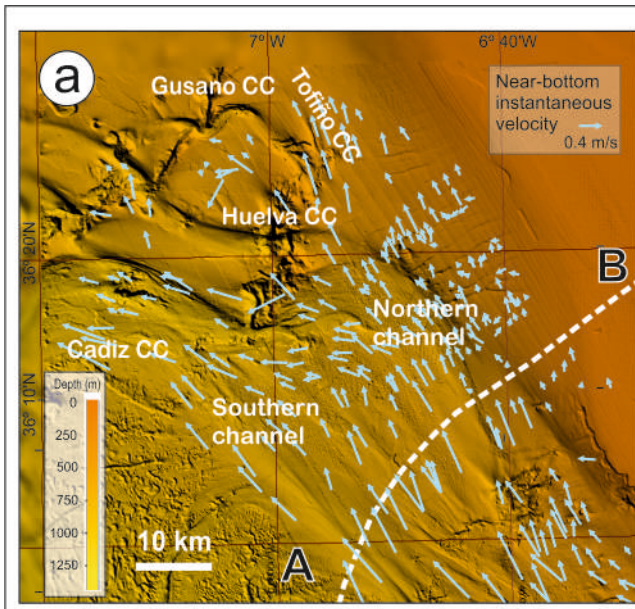
The authors declare that they have no known competing financial interests or personal relationships that could have appeared to influence the work reported in this paper.

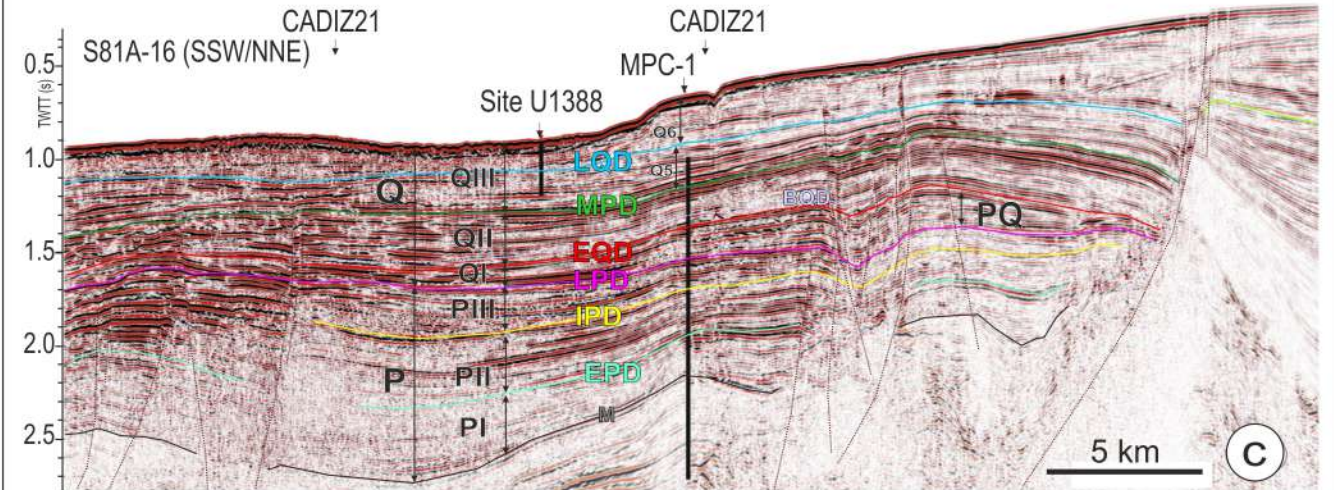
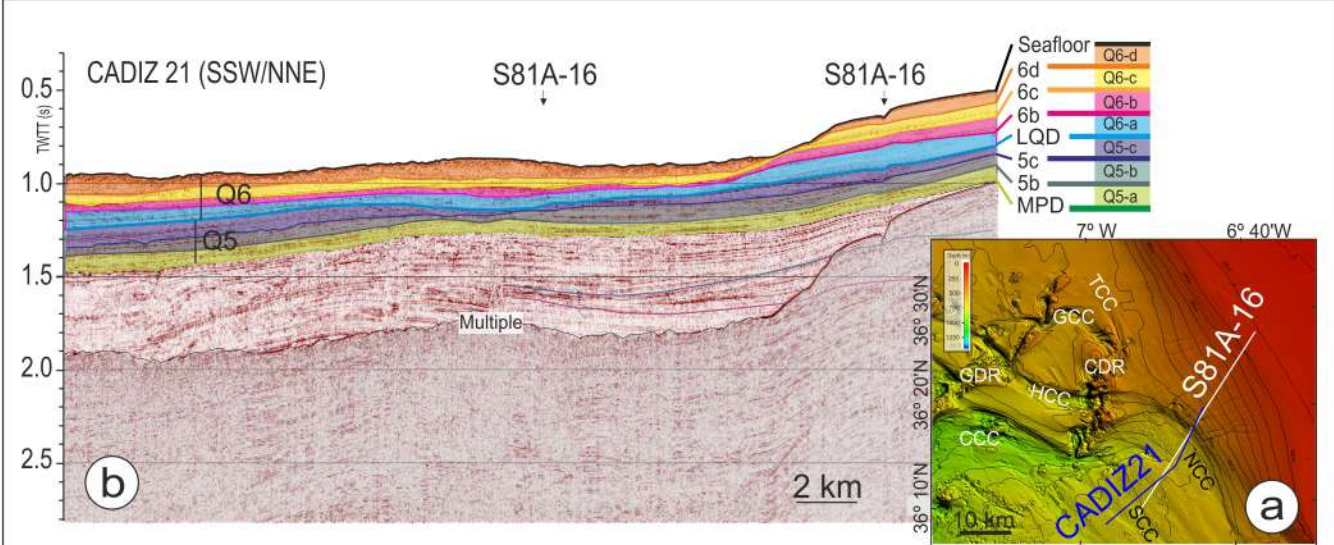
The authors declare the following financial interests/personal relationships which may be considered as potential competing interests:

Signed: Marga Garcia on behalf of all co-authors

Journal Pre-proof





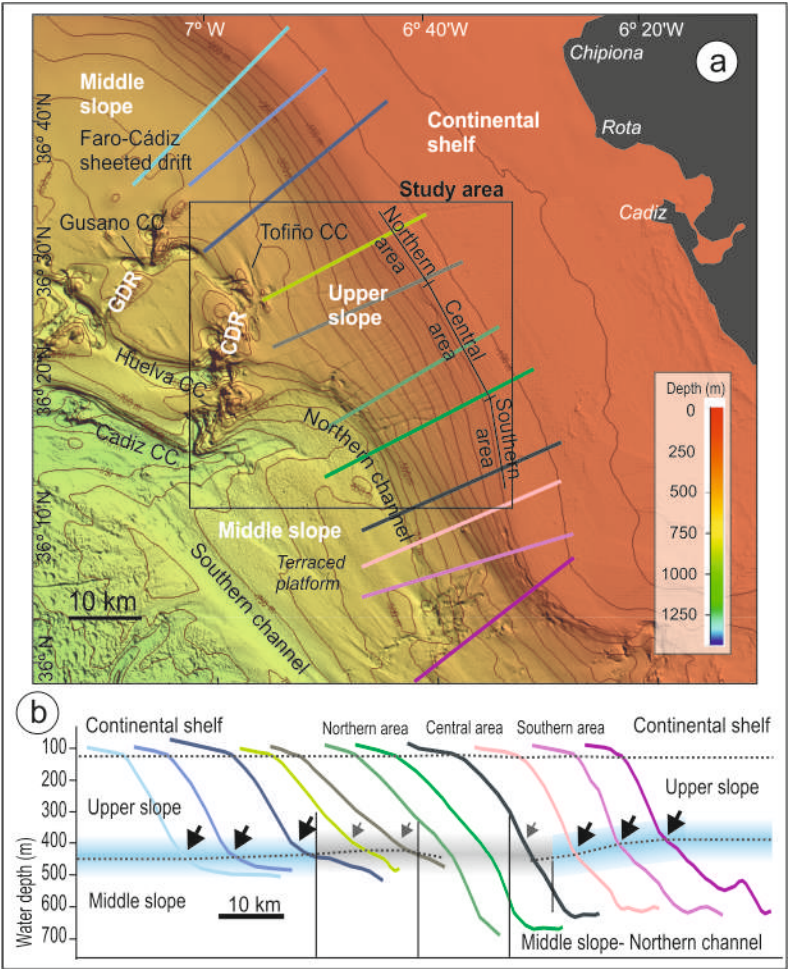


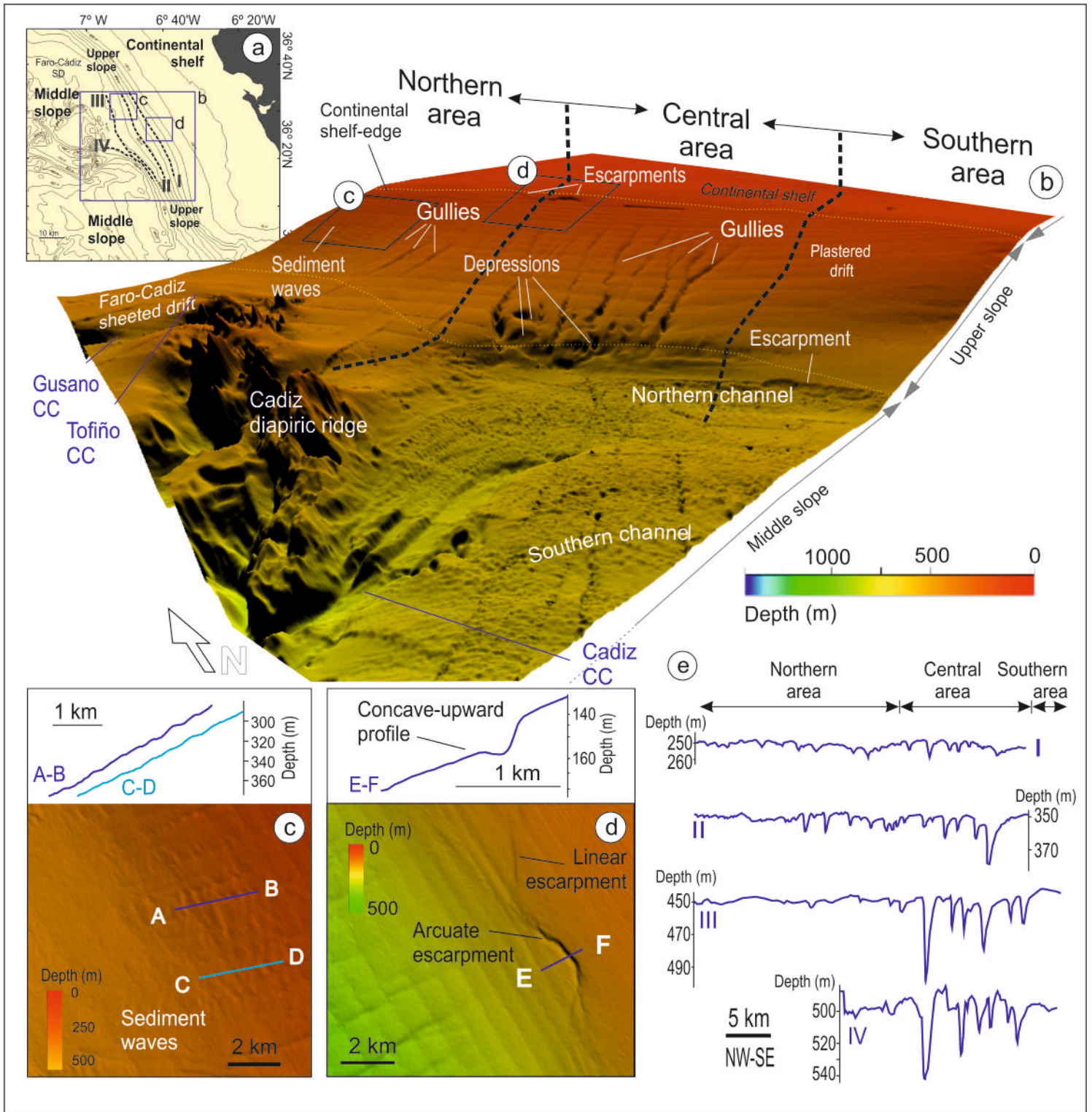
d

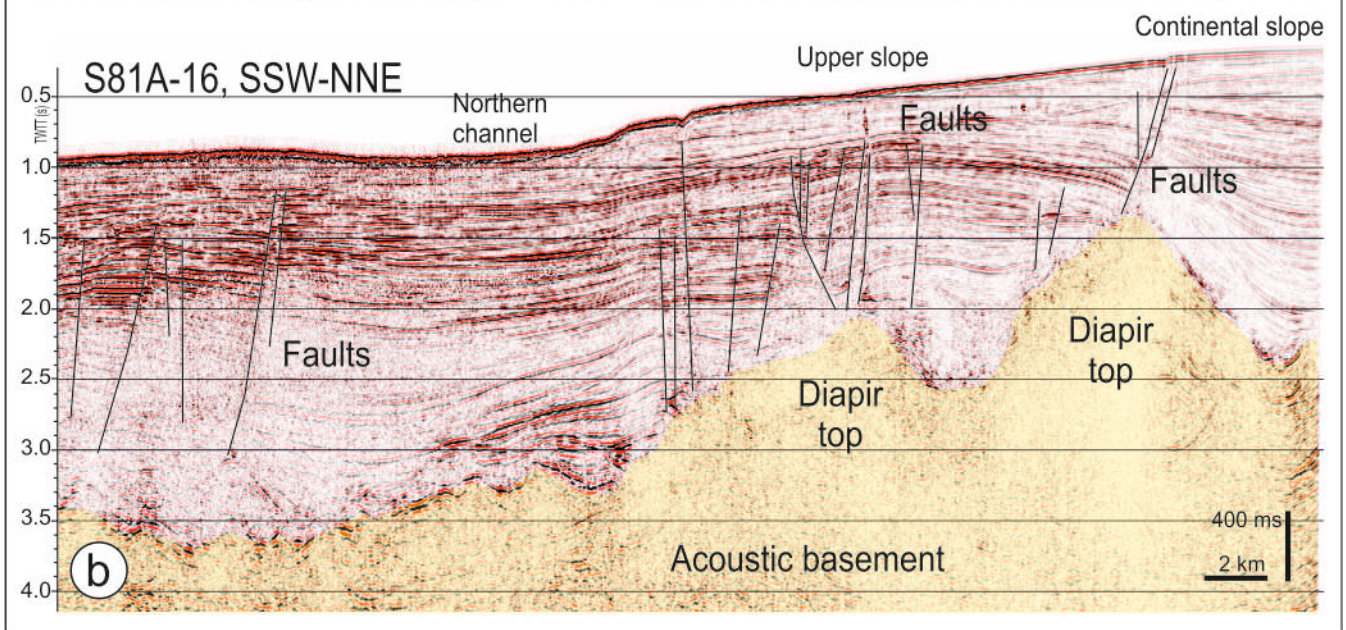
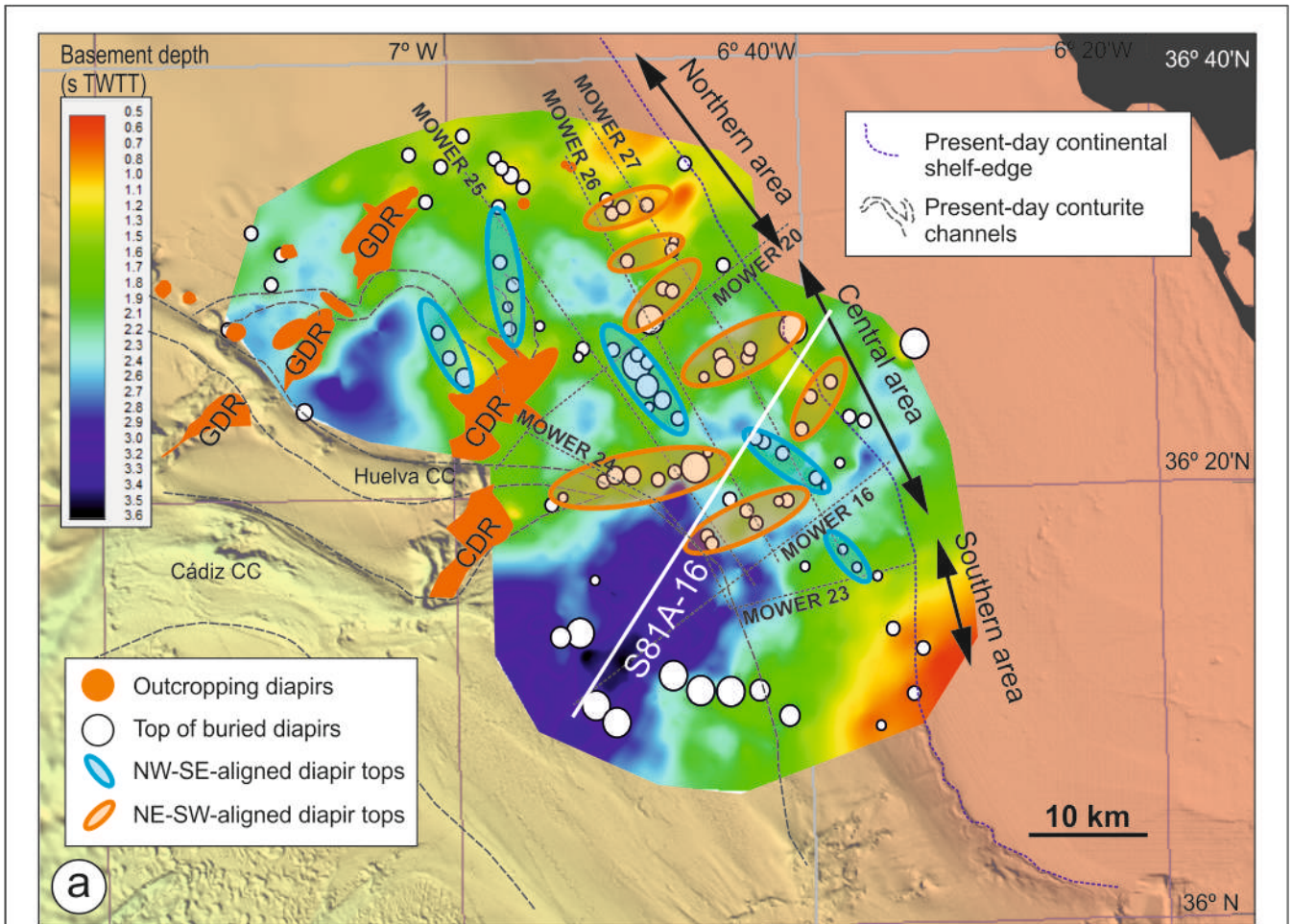
Stratigraphic Unit	Age (My)	Reference
Q6	0.001 - 0.002	Llave et al., 2001, 2007
Q5	0.002 - 0.006	Hernández-Molina et al., 2002, 2006
Q4	0.006 - 0.010	Marchés et al., 2010
Q3	0.010 - 0.011	Llave et al., 2011
Q2	0.011 - 0.012	Roque et al., 2012
Q1	0.012 - 0.013	Bracknidge et al., 2013
Q0	0.013 - 0.016	Hernández-Molina et al., 2016

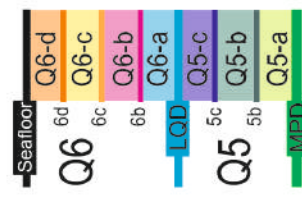
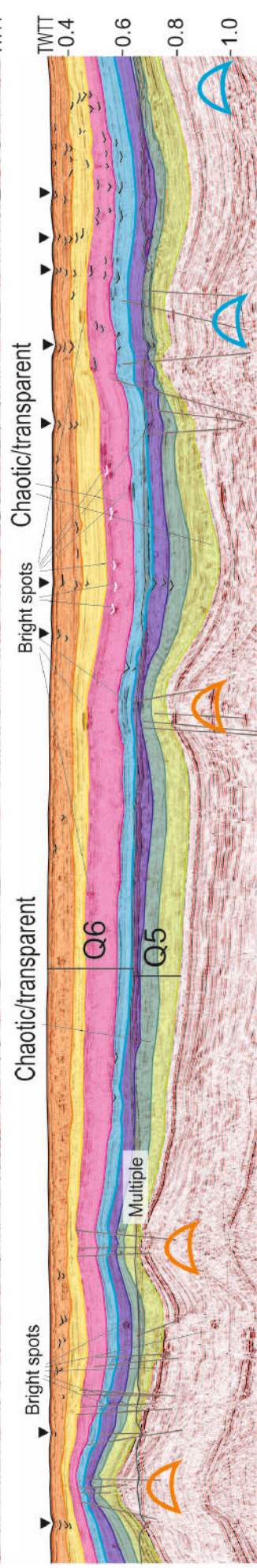
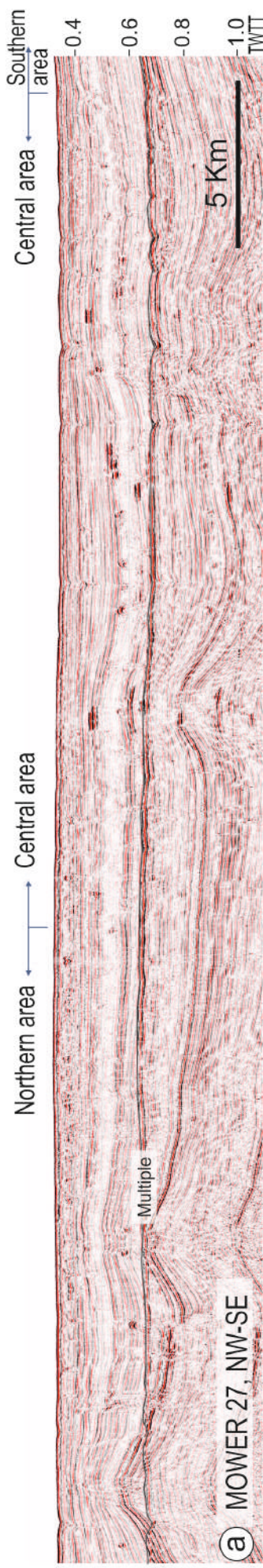
Unit	Sub-unit	Notes
Q6	Q6-d	Small in NA, NW migration SA
	Q6-c	Rare, associated to faults, SA
	Q6-b	All sub-unit in SA, top in NA
	Q6-a	All sub-unit in SA, top in NA
Q5	Q5-c	Rare, associated to faults, top of sub-units in Northern area
	Q5-b	Rare, associated to faults, top of sub-units in Northern area
	Q5-a	Rare, associated to faults, top of sub-units in Northern area
	MPD	

Depth (m)	Benthic $\delta^{18}O$ (per mil)	MIS
0	~3.5	1
10	~3.5	2
20	~3.5	3
30	~3.5	4
40	~3.5	5
50	~3.5	6
60	~3.5	7
70	~3.5	8
80	~3.5	9
90	~3.5	10
100	~3.5	11
110	~3.5	12
120	~3.5	13
130	~3.5	14
140	~3.5	15
150	~3.5	16
160	~3.5	17
170	~3.5	18
180	~3.5	19
190	~3.5	20
200	~3.5	21
210	~3.5	22
220	~3.5	23

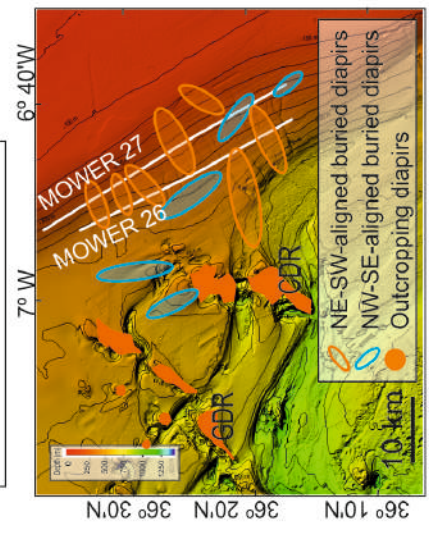
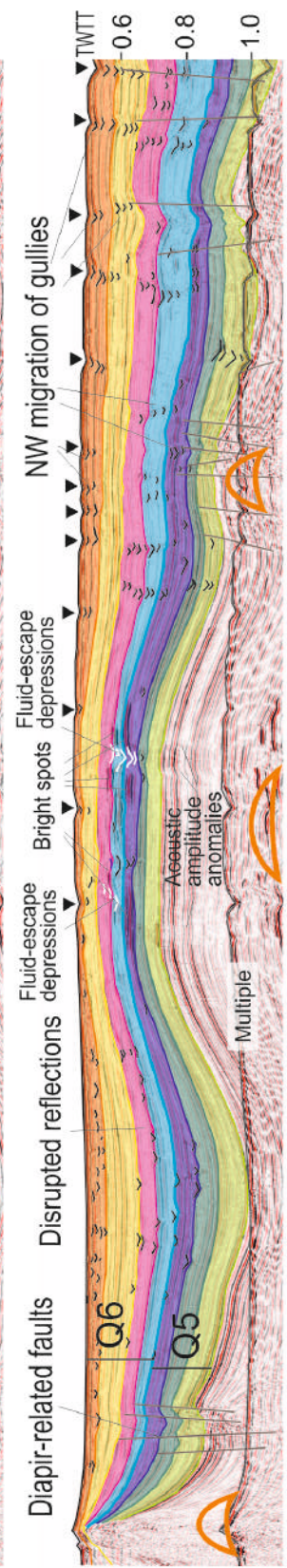
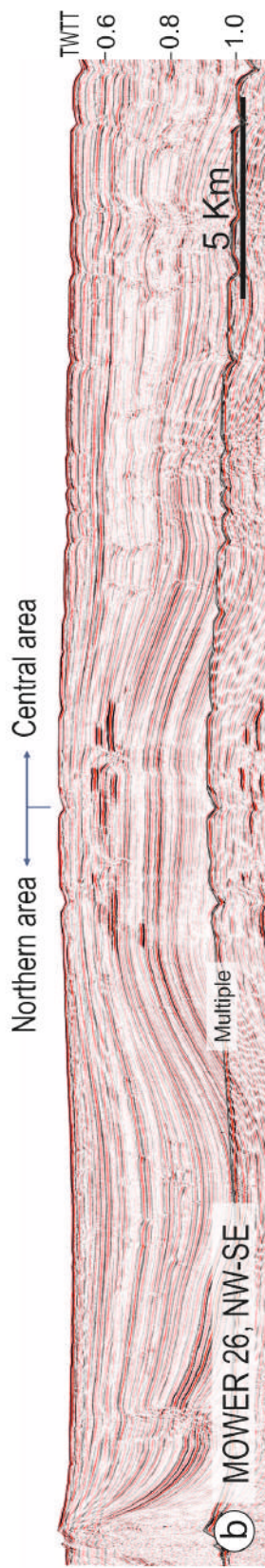


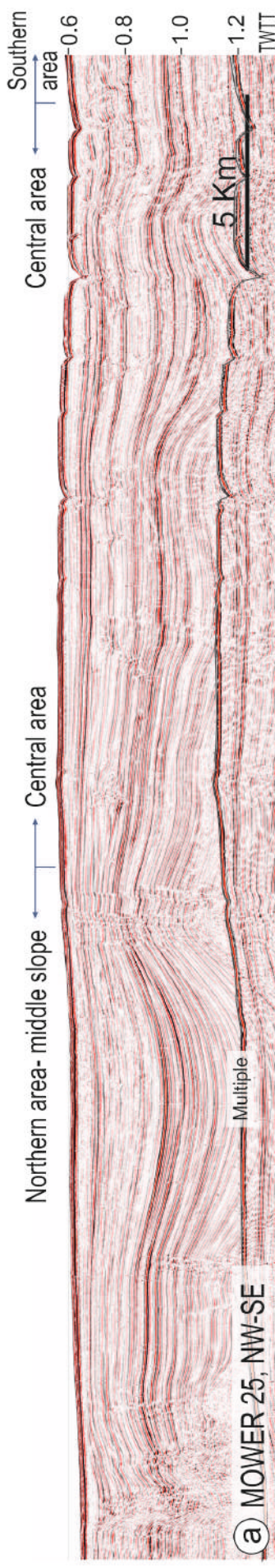




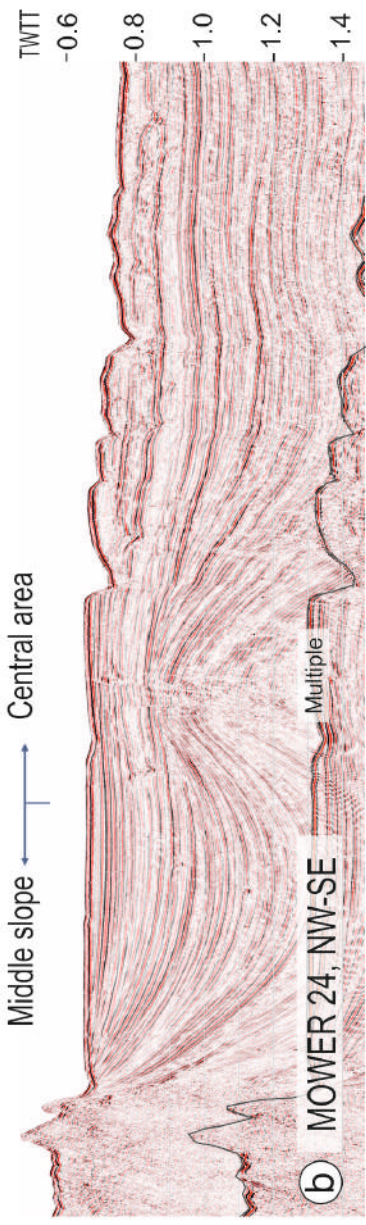
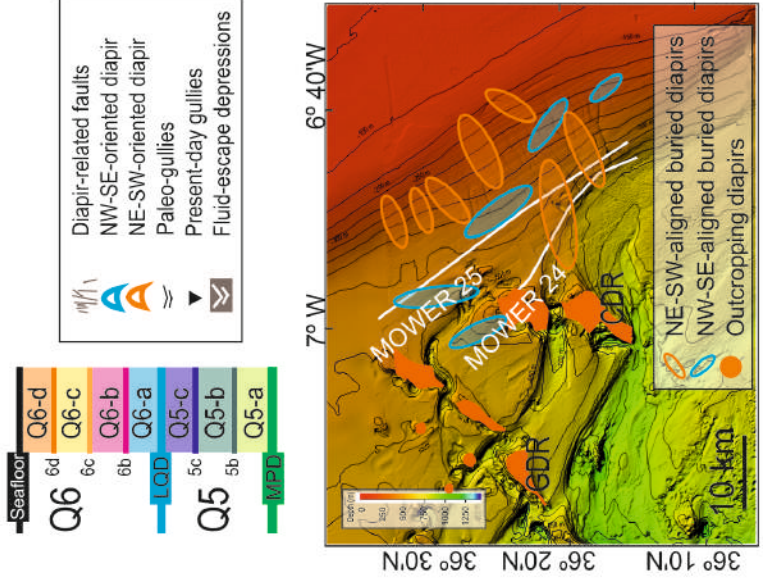
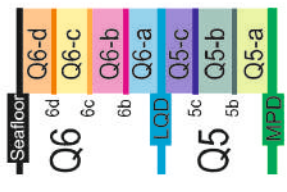
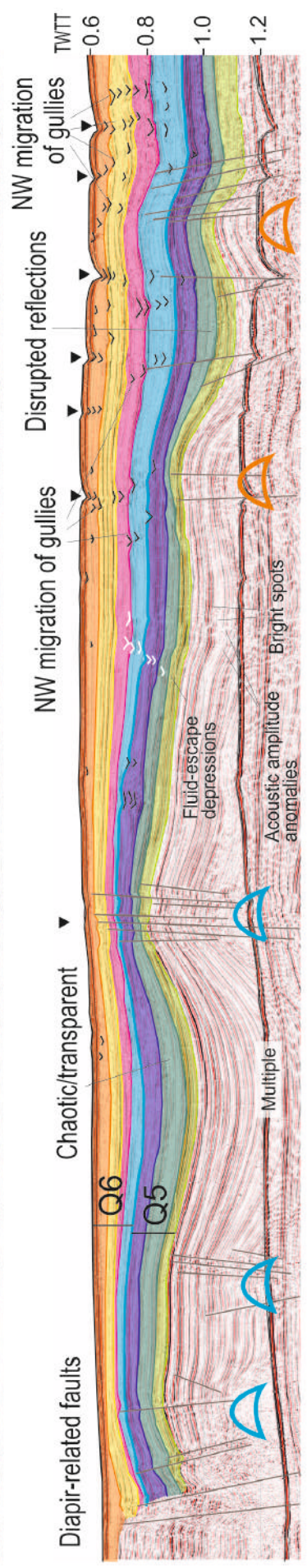


- Diapir-related faults
- NW-SE-oriented diapir
- NE-SW-oriented diapir
- Paleo-gullies
- Present-day gullies
- Fluid-escape depressions

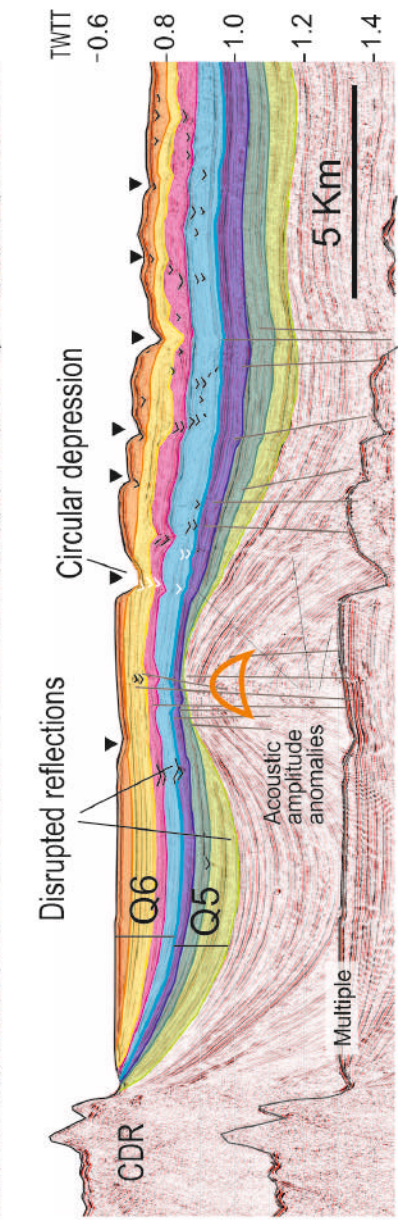


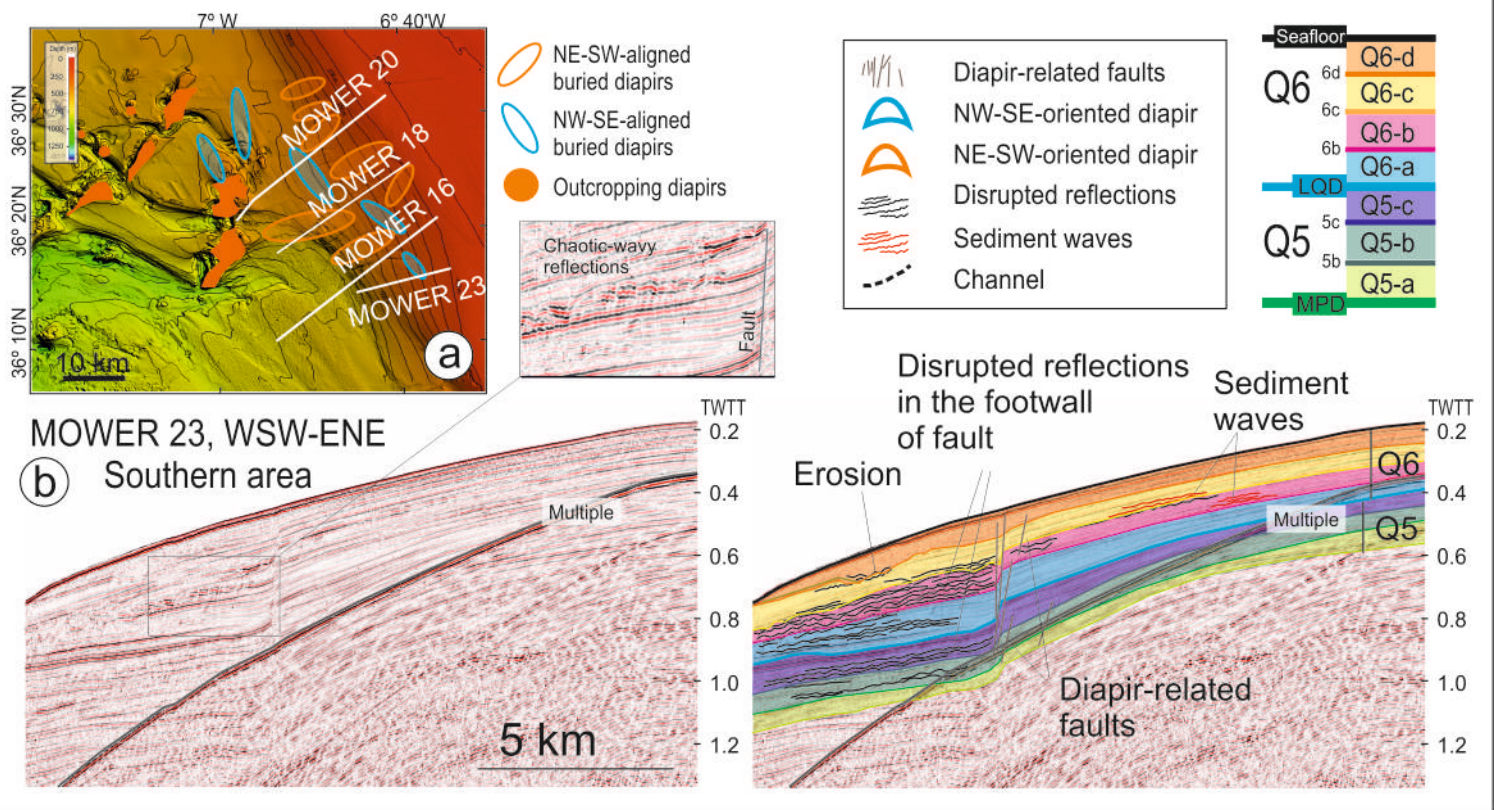


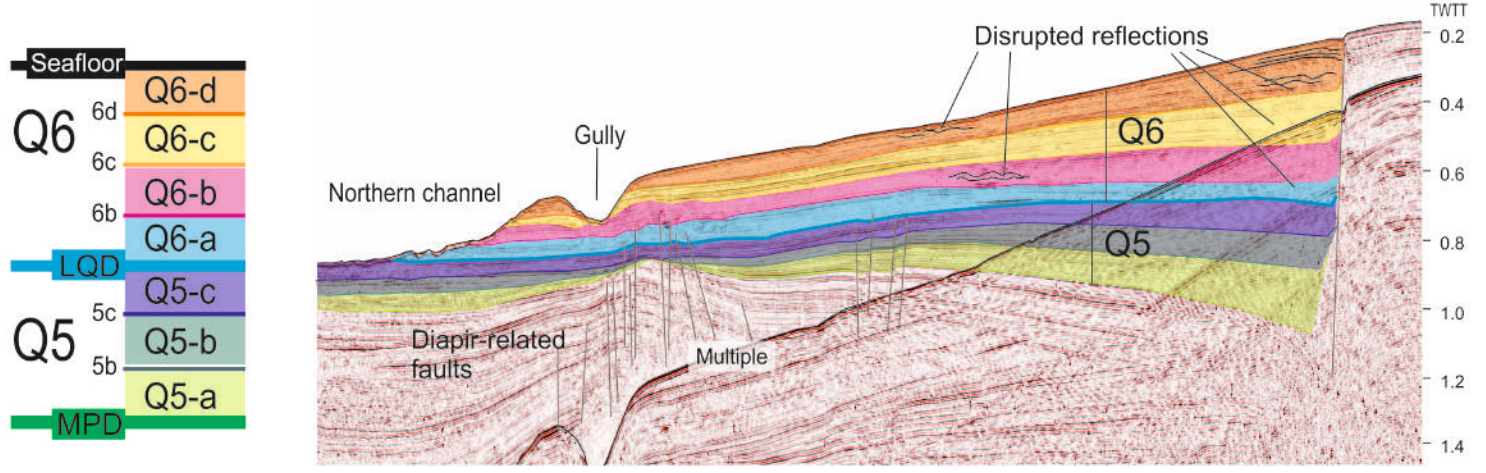
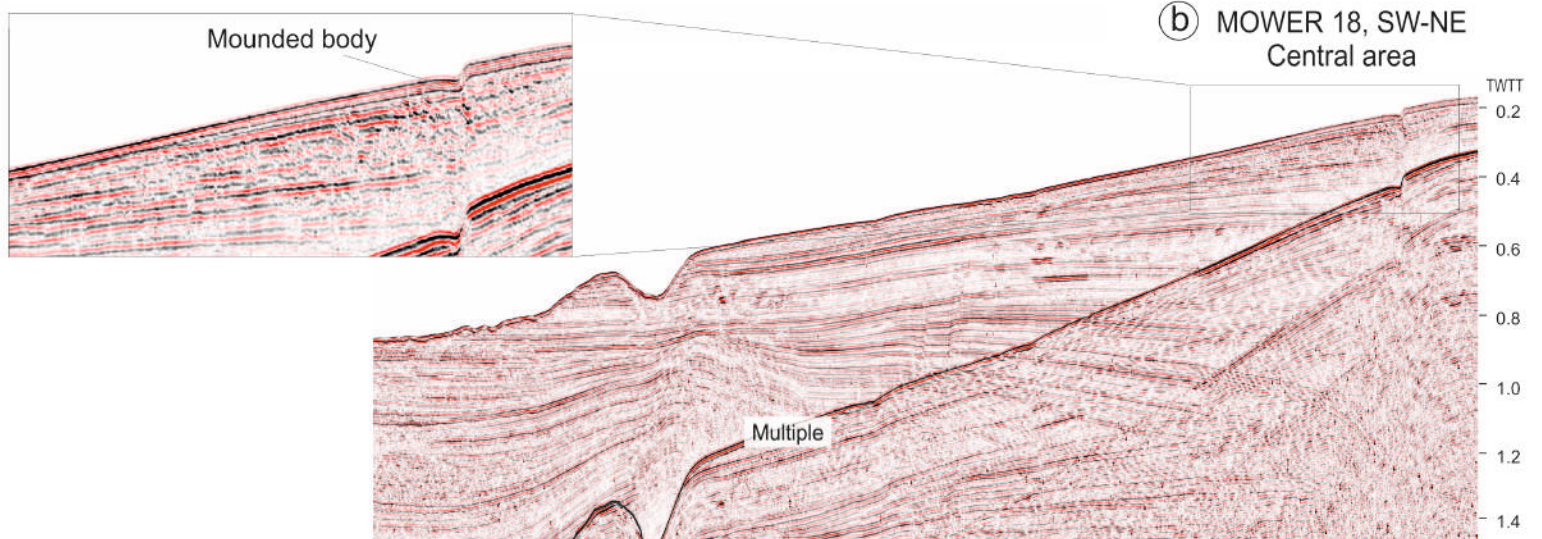
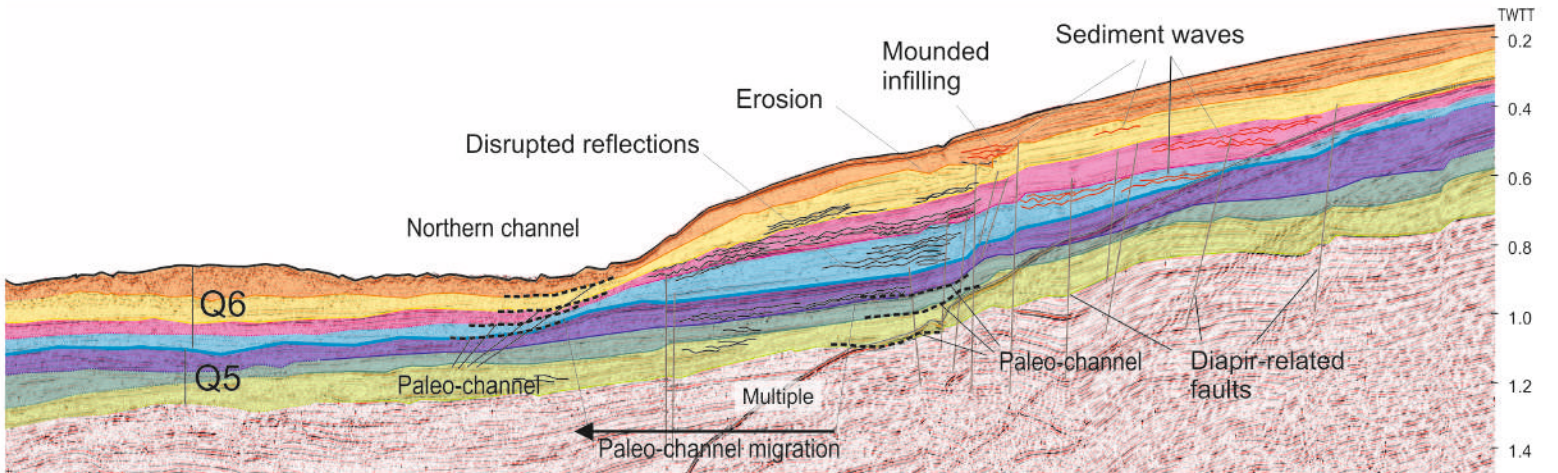
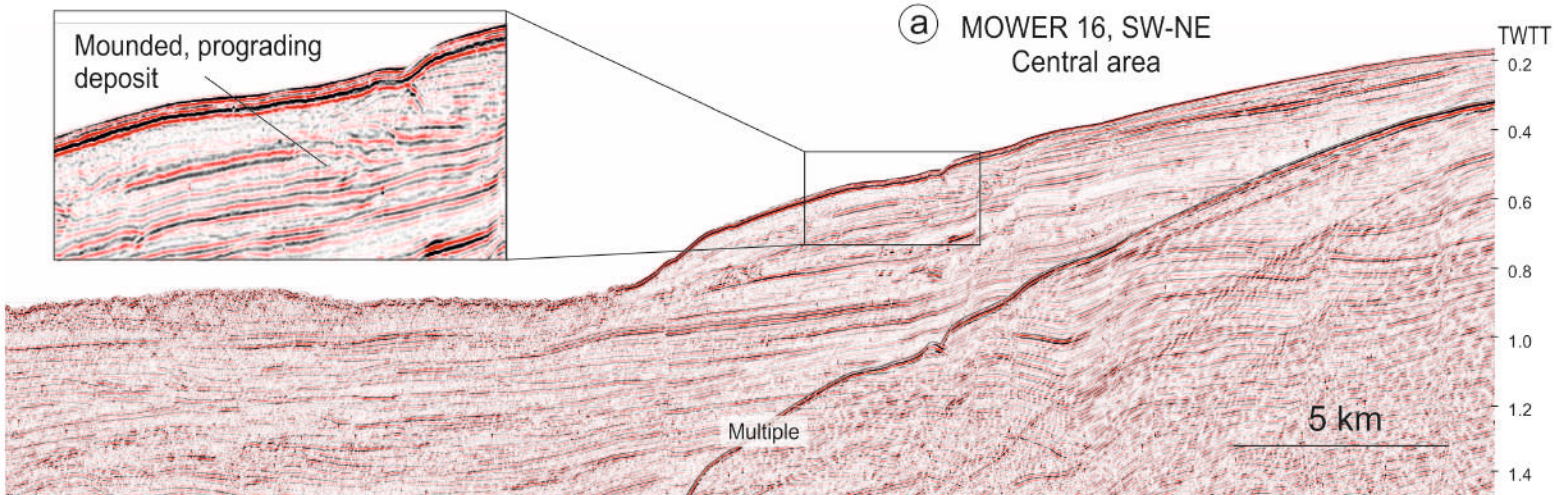
(a) MOWER 25, NW-SE



(b) MOWER 24, NW-SE

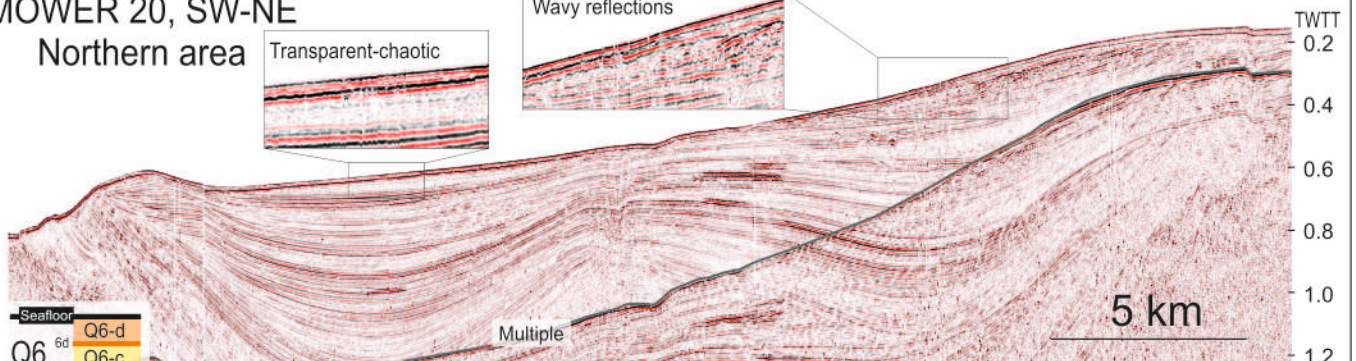
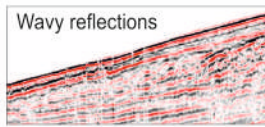
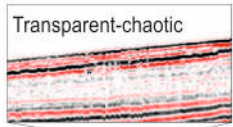






Seafoor	
Q6	6d Q6-d
	6c Q6-c
	6b Q6-b
	6a Q6-a
LQD	
Q5	5c Q5-c
	5b Q5-b
	5a Q5-a
MPD	

MOWER 20, SW-NE
Northern area



- Sea floor
- Q6
- 6d Q6-d
- 6c Q6-c
- 6b Q6-b
- 6a Q6-a
- Q5
- 5c Q5-c
- 5b Q5-b
- 5a Q5-a

HCC
Cadiz diapiric ridge

Sediment waves

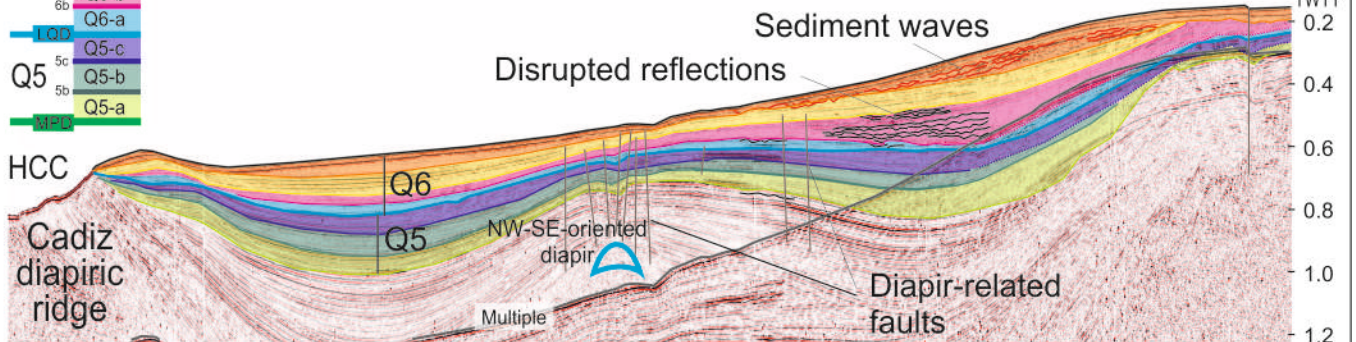
Disrupted reflections

NW-SE-oriented diapir

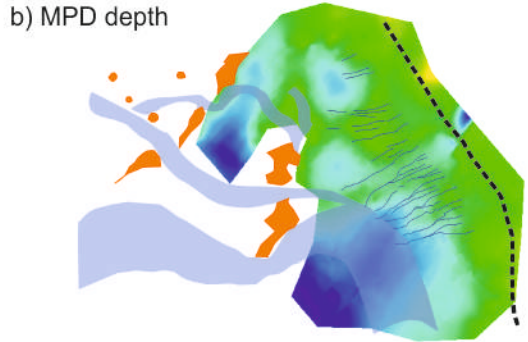
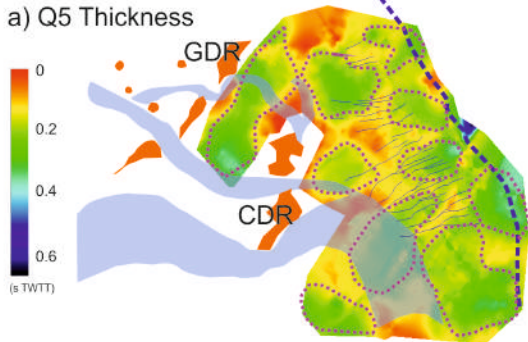
Diapir-related faults

Multiple

TWTT
0.2
0.4
0.6
0.8
1.0
1.2



Units base topography and thickness



Sub-units thickness

